

AN ABSTRACT OF THE THESIS OF

WARREN LEWIS WEBB for the DOCTOR OF PHILOSOPHY
(Name) (Degree)

in FOREST MANAGEMENT presented on _____
(Major) (Date)

Title: PHOTOSYNTHETIC RESPONSE MODELS FOR A
TERRESTRIAL PLANT COMMUNITY

Abstract approved: _____
Michael Newton

Photosynthetic response to light and temperature was modeled using data from a small red alder (Alnus rubra B.) community growing in a controlled environment chamber linked to the computer. This new system controls air temperature, root temperature, and vapor pressure over a wide range, and both light intensity and spectral quality are comparable with natural sunlight. Net photosynthetic rates are measured by continuously monitoring atmospheric CO₂ in the gas-tight environment chamber. Photosynthetic measurements were taken between 0.06 ly/min and 0.68 ly/min (total short-wave radiation) at temperatures from 6° to 30°C.

A stepwise multiple linear regression analysis accounted for 98% of the variation in steady-state net photosynthesis using light and temperature plus two interaction terms as independent variables. Non-linear models were constructed based on the known light curve for photosynthesis of single plants. The weighted average deviation of the

data from the best non-linear model was $\pm 3.7\%$. Extrapolation of predicted photosynthetic response appears reliable except for an inconsistency at light energies below 5% full sunlight for temperatures less than 6°C .

Photosynthetic Response Models for a
Terrestrial Plant Community

by

Warren Lewis Webb

A THESIS

submitted to

Oregon State University

in partial fulfillment of
the requirements for the
degree of

Doctor of Philosophy

June 1971

APPROVED:

Associate Professor of Forest Management

Head of Department of Forest Management

Dean of Graduate School

Date thesis is presented _____

Typed by Mary Jo Stratton for Warren Lewis Webb

ACKNOWLEDGEMENTS

Thanks are due many people for their help with my program and I regret the lack of space to thank them all. I would like to acknowledge the help of Drs. Joe Zaerr and Richard Waring for their critical review of this thesis, Drs. Logan Norris and Ian Tinsley for their assistance in preparing grant proposals, and Dr. George Brown for loaning me his laboratory and data acquisition system. Special thanks go to my major professor, Dr. Michael Newton, who gave me freedom to choose a thesis problem and provided encouragement and assistance throughout this project.

Thanks are due Dr. Brian Cleary, Weyerhaeuser Company, and Richard Holbo for their advice on equipment development and maintenance. My formulation of the photosynthetic response models were influenced greatly by discussions with Duane Starr, graduate student in Physical Chemistry. The Environmental Health Sciences Center provided a fellowship and funds to purchase the environment chamber used in this study.

And, most of all, thanks to my wife, M. Katherine.

TABLE OF CONTENTS

| | <u>Page</u> |
|--|-------------|
| INTRODUCTION | 1 |
| LITERATURE REVIEW | 2 |
| Photosynthetic Response Models | 2 |
| Light | 4 |
| Temperature | 6 |
| Light-Temperature Interactions of Photosynthesis | 8 |
| Plant Community Photosynthesis and Respiration | 9 |
| METHODS AND MATERIALS | 11 |
| Computer-Linked Controlled Environment System | 11 |
| Environment Chamber | 11 |
| Growth Medium Control | 19 |
| Carbon Dioxide Control and Measurement | 21 |
| Plant Community and Environmental Program | 24 |
| Experiment One | 25 |
| Experiment Two | 25 |
| Experiment Three | 28 |
| RESULTS AND DISCUSSION | 31 |
| Experiment One | 31 |
| Experiment Two | 33 |
| Stepwise Multiple Linear Regression Models | 33 |
| Non-linear Structural Response Model | 37 |
| Experiment Three | 56 |
| CONCLUSIONS | 60 |
| BIBLIOGRAPHY | 62 |
| APPENDIX | 65 |

LIST OF TABLES

| <u>Table</u> | | <u>Page</u> |
|--------------|---|-------------|
| 1 | Summary of first stepwise analysis. | 34 |
| 2 | Summary of second stepwise analysis. | 35 |
| 3 | Summary of third stepwise analysis. | 36 |
| 4 | Parameters from equation (6) for five radiation levels. | 40 |
| 5 | Energy distribution between visible and infrared spectra of xenon arc. | 70 |
| 6 | Short-wave radiation transmission of xenon arc for several filter combinations, 18" from floor. | 73 |
| 7 | Radiation uniformity in the environment chamber. | 74 |
| 8 | Temperature uniformity in the environment chamber. | 75 |
| 9 | Air velocities in chamber. | 78 |
| 10 | Nutrient solution used for red alder. | 78 |

LIST OF FIGURES

| <u>Figure</u> | | <u>Page</u> |
|---------------|---|-------------|
| 1 | Generalized light curve for net photosynthesis. | 5 |
| 2 | Computer-linked controlled environment system. | 12 |
| 3A | Xenon arc spectrum with IR absorbing inner filter and quartz outer filter. | 14 |
| 3B | Infrared spectrum of xenon arc with inner IR filter and outer quartz filter. | 15 |
| 4 | Controlled environment chamber, side view. | 17 |
| 5 | Controlled environment chamber with chemical dehumidification system, top view. | 18 |
| 6 | Nutrient control system. | 20 |
| 7 | Environment chamber accessories. | 22 |
| 8 | CO ₂ measuring and control system. | 23 |
| 9 | Daily short-wave radiation pattern of alder community, experiment 1. | 26 |
| 10 | Temperature time curve for experiment 3. | 29 |
| 11 | Radiation time course for experiment 3. | 30 |
| 12 | Light curve for red alder community. Experiment 1. | 32 |
| 13 | Generalized light curve. | 38 |
| 14 | Generalized Psn response to temperature. | 39 |
| 15 | Net photosynthetic response to temperature of five radiation levels. | 41 |

| <u>Figure</u> | | <u>Page</u> |
|---------------|--|-------------|
| 16 | Maximum photosynthetic response to temperature at five light levels. | 42 |
| 17 | Temperature of maximum photosynthetic response for five light levels. | 43 |
| 18 | Slope coefficient from temperature response equation (3) for five light levels. | 44 |
| 19 | Estimation of respiration as function of temperature. | 46 |
| 20 | Photosynthetic response to light and temperature. | 47 |
| 21 | Photosynthetic response to light and temperature. | 48 |
| 22 | Frequency distribution of residuals for equation (8). | 50 |
| 23 | Frequency distribution of residuals, equation (9). | 51 |
| 24 | Photosynthetic response to light and temperature. | 52 |
| 25 | Photosynthetic response to light and temperature. | 54 |
| 26 | Frequency distribution of residuals for equation (10). | 55 |
| 27 | Frequency distribution of relative residuals for equation (12). | 57 |
| 28 | Net photosynthesis. | 58 |
| 29 | Comparison between stepwise and non-linear models as predictors of photosynthesis. | 59 |
| 30 | Xenon arc spectra at 12", 18", and 24" from floor, center of chamber. | 68 |

| <u>Figure</u> | | <u>Page</u> |
|---------------|--|-------------|
| 31 | Xenon arc spectrum 12" from floor near one end of chamber. | 69 |
| 32 | Radiation transmission spectra of xenon arc for white and grey filters. | 71 |
| 33 | Spectra transmission for several chamber filters. | 72 |
| 34 | Comparison of actual chamber temperature and the temperature pattern programmed onto the cam programmer. | 76 |
| 35 | Comparison of chamber wet bulb depression with pattern programmed on cam programmer. | 77 |
| 36 | Record of CO ₂ depletion and resupply in environment chamber. | 79 |

PHOTOSYNTHETIC RESPONSE MODELS FOR A TERRESTRIAL PLANT COMMUNITY

INTRODUCTION

Green plants function as the major producers of reduced carbon for all living systems. There has been a great deal of recent interest in analytical modeling of this primary production process. Such models would provide estimates of constraints to primary productivity necessary for sound decisions in vegetation management. Models of primary productivity would also help in understanding the effect of perturbations on the natural system such as irrigation, fertilization, or air contamination.

Since primary productivity is responsive to the plant's physical environment, a general prediction model should include environmental variables. Fortunately, many investigators have studied plant response to single environmental variables in terms of net photosynthesis, the time derivative of primary productivity. These investigations form a sound conceptual basis for modeling the photosynthetic response of small plant communities in terms of environmental variables.

Models of net photosynthesis controlled by light and temperature of a small red alder community are presented in this thesis. A new controlled environment system linked to the computer has been used to collect the data for validation.

LITERATURE REVIEW

Photosynthetic Response Models

The prediction of dry matter accumulation, based on photosynthetic and respiratory data, has received a great deal of attention recently. Several authors (Cleary, 1971; Larcher, 1969; Ledig, 1969) have proposed mathematical models relating photosynthesis to growth. All models have a great deal of merit, but most of them suffer from insufficient data either to verify the model or evaluate its coefficients.

Cleary's response model is of the general form:

$$\text{Response} = P_s = f(M, T, L, N, \dots)$$

P_s = Photosynthesis

M = Moisture

T = Temperature

L = Light

N = Nutrients

By taking the partial derivative of the response to each environmental variable and adding the appropriate error terms, the model becomes:

$$dR = \left(\frac{\partial R}{\partial M}\right)dM + \left(\frac{\partial R}{\partial T}\right)dT + \left(\frac{\partial R}{\partial L}\right)dL + \dots$$

This additive response model must be used to predict photosynthetic response per unit of plant material since the equation has no component for plant growth. Without this feature, the model does not consider the changing response per plant due to such factors as

shading of lower leaves as upper leaves develop.

Ledig's model (Ledig, 1969; Ledig and Perry, 1969) is a differential equation expressing dry weight accumulation as a function of photosynthesis and leaf weight, both of which are written as functions of time. This model considers the change in photosynthetic efficiency with season and the translocation of photosynthates to various plant parts.

$$\frac{dY(t)}{dt} = KP(t)a(Y(t))^b$$

$Y(t)$ = dry weight as function of time

$P(t)$ = photosynthetic rate as function of time

$L(t) = a(Y(t))^b$ = leaf dry weight as function of time

K = dry weight/ CO_2 weight

The function $K(P(t))$ is equivalent to net assimilation rate (NAR) which is equal to the change in dry weight per unit time per unit leaf area.

The function $L(t)$ is determined using the allometric relation between leaf weight and total dry weight. The constants (a, b) are determined for each species and each set of growing conditions.

This model illustrates the importance of photosynthetic rates and photosynthetic movement in modifying dry weight accumulation. The model was validated under the same experimental conditions that were used to derive the functions $K(P(t))$ and $L(t)$ and does not incorporate photosynthetic response to changes in environmental variables.

A great deal of information is available in the literature on the environmental effects on photosynthesis of single plants. The effects of light, temperature, water potential, and ambient CO₂ concentrations have been emphasized in connection with photosynthesis. In general, ambient concentrations of CO₂ in the field do not vary significantly, but increasing plant moisture stress (or decreasing water potential) decreases photosynthesis. The latter is a significant factor in the growth of wildland species and should be included in a completed predictive model. Maximum growth occurs during periods of low plant moisture stress. Growth during period of low stress is therefore a strong function of light and temperature (Gaastrri, 1963)-- the two variables evaluated in this review.

Light

The German botanist, J. Reinke, in 1883 was the first to note the light saturation phenomenon of photosynthesis (Rabinowitch, 1969) (Figure 1). However, it remained for F. F. Blackman in 1905 to interpret the shape of the curve as a two-step mechanism consisting of an initial photochemical step followed by a temperature-controlled dark step (Heath, 1969). Since that time, many investigators have expanded the interpretation of this basic physiological phenomenon.

The light energy at which net photosynthesis (P_{sn}) is zero is termed the compensation point (Gaastrri, 1963; Heath, 1969; Kramer,

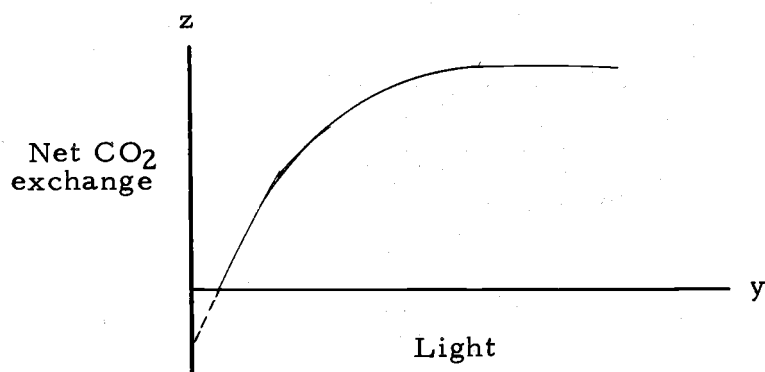


Figure 1. Generalized light curve for net photosynthesis.

1960; Rabinowitch, 1951). This is the point of zero CO₂ exchange between the plant surface and the atmosphere and may vary widely with climatic conditions, species, and various light-adaptive features (Gaastrri, 1963). The initial part of the curve, which is nearly linear, represents the photochemical reaction in photosynthesis (Heath, 1969; Rabinowitch, 1969). This function determines the maximum quantum yield, has a Q_{10} nearly equal to one, and varies only slightly for different species and different environmental conditions (Gaastrri, 1963). This linear portion can be extrapolated through the compensation point to zero light intensity and the intercept value interpreted as a measure of respiration.

Photosynthetic rates in the saturated region of the curve are independent of light and dependent upon factors that influence the dark reactions of photosynthesis (Rabinowitch, 1956). Thus, photosynthesis in this region is strongly dependent upon temperature, water

potential, species, specimen, and many internal factors, the most important of which appears to be adaptation to strong or weak light. Decreasing photosynthetic rates at strong light intensities are often indicative of irreversible damage to the chloroplasts. Also, the increased radiation load may affect other biochemical processes resulting in decreased photosynthesis.

Between the light-dependent and light-independent regions of the curve occurs a "transition" zone. Some workers feel that a diffusion limited process occurs in this region of the curve since the measured Q_{10} value of 1.1 is higher than a light-dependent value of 1.0 but lower than a temperature dependent process of 2.0 to 3.0 (Gaastrri, 1963).

Temperature

The temperature range for reversible photosynthesis in many plants is between 0 and 30°. At less than 5° a slow chill damage can occur, and at greater than 25° the photosynthesis apparatus may be irreversibly damaged by heat (Rabinowitch, 1956). At extreme temperatures, then, photosynthesis becomes a function of time and temperature. In the range between 5 and 25°, photosynthesis is independent of time and often can be predicted from the Arrhenius function.

$$P = A \exp \left(\frac{B}{T} \right)$$

P = photosynthesis

T = °K

A, B = constants

This function is nearly linear over a small range of temperature because temperature is expressed in degrees Kelvin. However, net photosynthesis does not follow this linear relationship but more closely approximates some curvilinear function between 0 and 40°C. Recent data by Austrian workers (Pisek, 1969) have shown that the rise and corresponding decline of net photosynthesis from 0 to 40°C is symmetric about some intermediate temperature at which photosynthesis is maximum. Expressing their data on a relative basis, they were able to show that this functional relationship held for many species during both the winter and summer. Strain (1966) found the same general function for some woody desert perennials. Again, some caution is advised in utilizing this function for high temperature response where irreversible heat injury may cause enzyme deactivation (Belehradek, 1957; Langriege, 1963).

Respiration at temperatures between 5 and 30°C can often be predicted from the linear Van't Hoff relationship with Q_{10} values ranging from 2 to 3 (Forward, 1960; Lewis, 1970). Some workers have found that respiration may increase in a slightly exponential manner up to 45 to 50°C (Strain and Chase, 1966). Blackman has proposed a qualitative relationship in which respiration increases

exponentially until certain critical temperatures are reached whereafter it declines as a function of time; the higher the temperature, the more negative is the time coefficient of respiration.

Light-Temperature Interactions of Photosynthesis

Except for the linear part of the light curve, all other properties of the curve have temperature coefficients. Light energy at the compensation point increases with temperature. This is because respiration increases with temperature and photosynthesis is independent of temperature at low light energies (Heath, 1969). Since the linear coefficient for the light curve is temperature independent while the compensation point is temperature dependent, the photosynthetic intercept point at zero light intensity would logically become more negative (an increase in respiration) as temperature increases. Many workers have found this to be true. The asymptotic value for photosynthesis in the light saturation region of the curve is strongly dependent upon temperature (Kramer and Kozlowski, 1960; Stalfelt, 1960). Most workers have shown an increase in photosynthesis in strong light as temperature is increased, but a decrease in net photosynthesis will undoubtedly occur at higher temperatures (Moir, 1969; Schulze, 1970). Stalfelt (1960) has shown that increasing light levels increase the temperature at which net photosynthesis is maximum. Milner (1969) found that clones of Mimulus required higher

light intensities to reach photosynthetic saturation as temperature increased. The relation was found to be essentially linear.

Plant Community Photosynthesis
and Respiration

A group of plants may respond differently to light than does a single plant. Light energy at various strata within the vegetation canopy is often predicted from the exponential relationship (Loomis et al., 1967; Saieki, 1963):

$$I = I_0 e^{-KF}$$

where

F = cumulative LAI

LAI = leaf area index = (leaf area/soil area)

K = extinction coefficient; function of community type, e. g.,
herbs, grasses, forest

I = radiation

I_0 = incident radiation at canopy surface

Interpreting this relationship qualitatively suggests that the inner leaves of a forested canopy may only reach the compensation point while the outer leaves of the canopy are exposed to full sunlight (Kramer and Kozlowski, 1960; Saieki, 1963). Therefore, the light saturation region of the photosynthetic light curve for a dense plant community may never be reached. Also, the transition range generally covers much higher light intensities than for single plants.

For example, single alfalfa leaves were found to reach photosynthetic saturation at 0.12 langley's/minute while an alfalfa crop reached light saturation at 0.45 langley's/minute (Gaastrri, 1963).

The daily photosynthetic rates for communities with closed canopies usually follow the diurnal radiation. Various workers have attempted to simulate community photosynthesis for a single species using the light saturation curve, various parameters characterizing solar radiation, and community parameters such as leaf area index and the spatial arrangement of the leaves in the community (Loomis, 1967; Saieki, 1963). The simulation works relatively well for solar radiation if one considers the light adaptation of the lower leaves in the canopy to low radiation. The simulation is less successful for periods of diffuse radiation.

The reported respiration rate of leaves is from 5 to 10% of gross photosynthesis at saturating light intensities. Daily respiration of whole plants and of plant communities is a much larger fraction of gross photosynthesis than for single leaves. Gaastrri (1963) found the total respiration of alfalfa to be between 35 and 49% of gross photosynthesis and for sugar beets the fraction was between 29 and 33%.

METHODS AND MATERIALS

Photosynthetic measurements were made on a small red alder community growing within a closed, controlled environment system assembled by the author and linked to the computer. These data were used as the foundation for constructing response models of photosynthesis to light and temperature. A description of the system including the Mallory environment chamber follows.

Computer-Linked Controlled Environment System

The system consists of four sub-systems labeled A through D on Figure 2, p. 12. System A is the nutrient cycling system for maintaining an aerated solution at constant temperature, system B is the environment chamber per se, system C controls the level of carbon dioxide in the chamber, and system D is the CO₂ measuring system. The sub-systems are detailed in successive diagrams (Figures 4, 5, 6, 7, 8). Data relating to the capability of the system and the methodology used to determine this capability are listed in the Appendix.

Environment Chamber

The environment chamber has a growth compartment of 4' x 2.5' x 4' and overall dimensions of 6'7" x 3' x 8'. The closed chamber has a

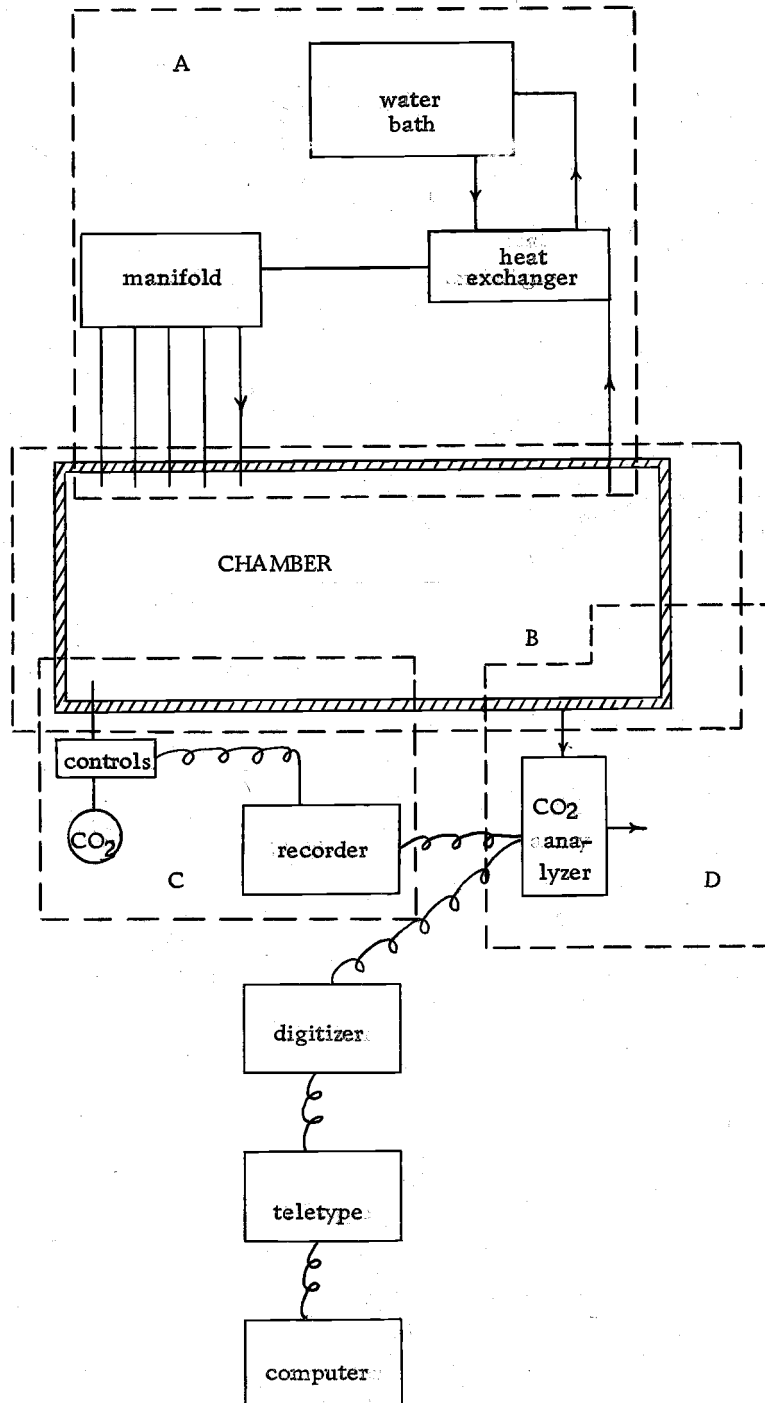


Figure 2. Computer-linked Controlled Environment System

maximum CO₂ leak rate of 0.1 ppm/minute across a gradient of 80 ppm with a driving force of 1.0 cm of water pressure. The leak rate across a 30 ppm gradient, which was the existing gradient under all measurement conditions, was .025 ppm/minute. The pressure gradient between the atmosphere and the chamber was maintained at \pm 3 mm of water pressure with the pressure regulating device shown in Figure 7.

Light Source. Light energy, comparable in intensity and quality to natural sunlight, was supplied with a single, water-cooled, 6000-watt xenon arc. (See light spectra, Figures 3A and 3B (Atlas, 1969).) The arc is jacketed with an infrared absorbing inner filter and a quartz outer filter. Distilled water was circulated through both filters with tygon tubing and cooled with tap water circulating through a stainless steel coil.

The walls and ceiling of the chamber are surfaced with stainless steel to maintain a high light intensity by reflection. A stainless steel reflector is positioned above the arc to give uniform light energy in the horizontal plane of the chamber. Power to the lamp is monitored with a watt meter and adjusted between 5500 and 6500 watts with an 11-tap transformer to maintain constant radiation as the arc ages. A 24-hour timer controls the on-off cycle.

Light Energy Control. Light energy reaching the plant canopy is modified by two retractable polyester fiberglass screens, each of

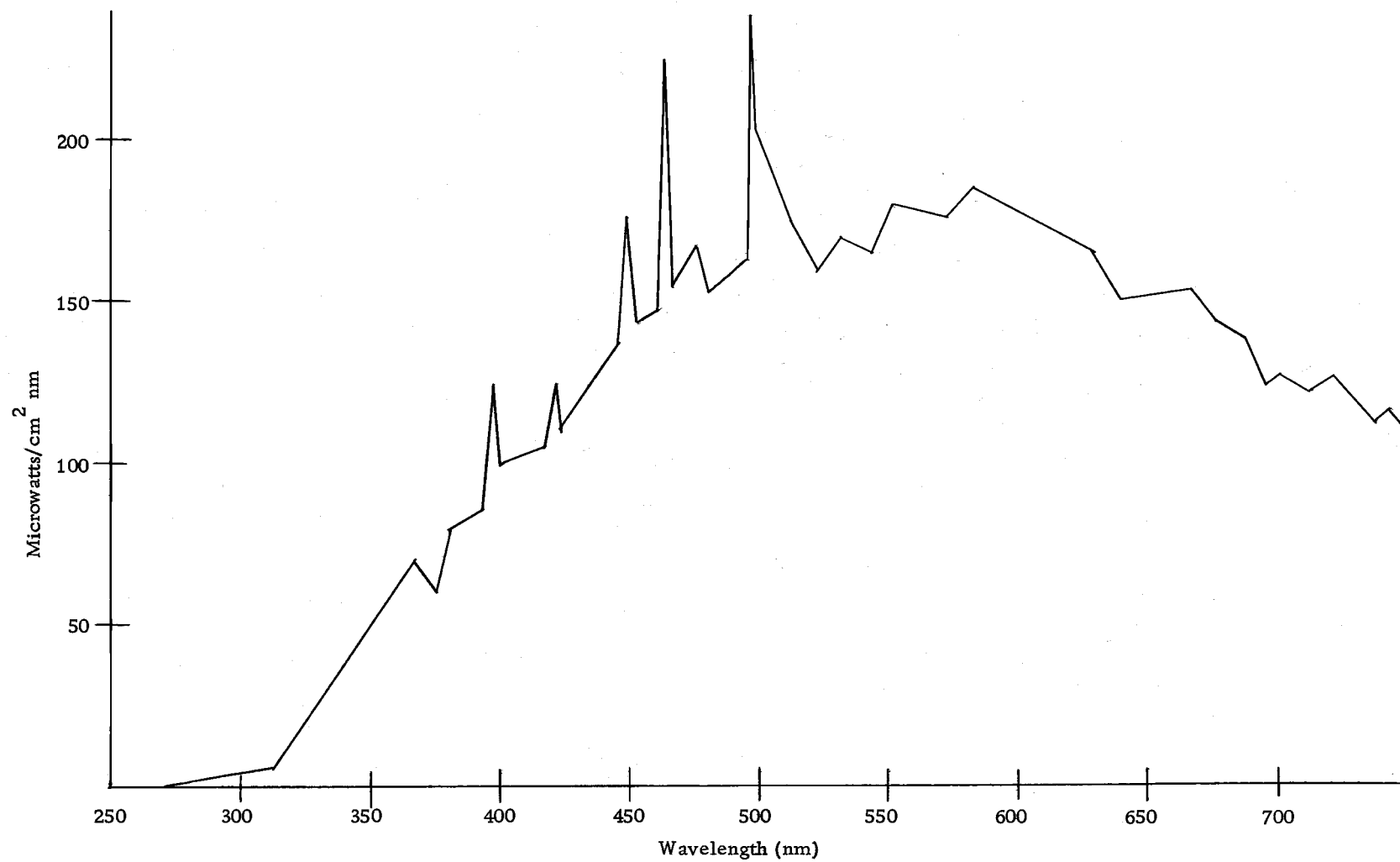


Figure 3A. Xenon arc spectrum with IR absorbing inner filter and quartz outer filter; 1 nm resolution.

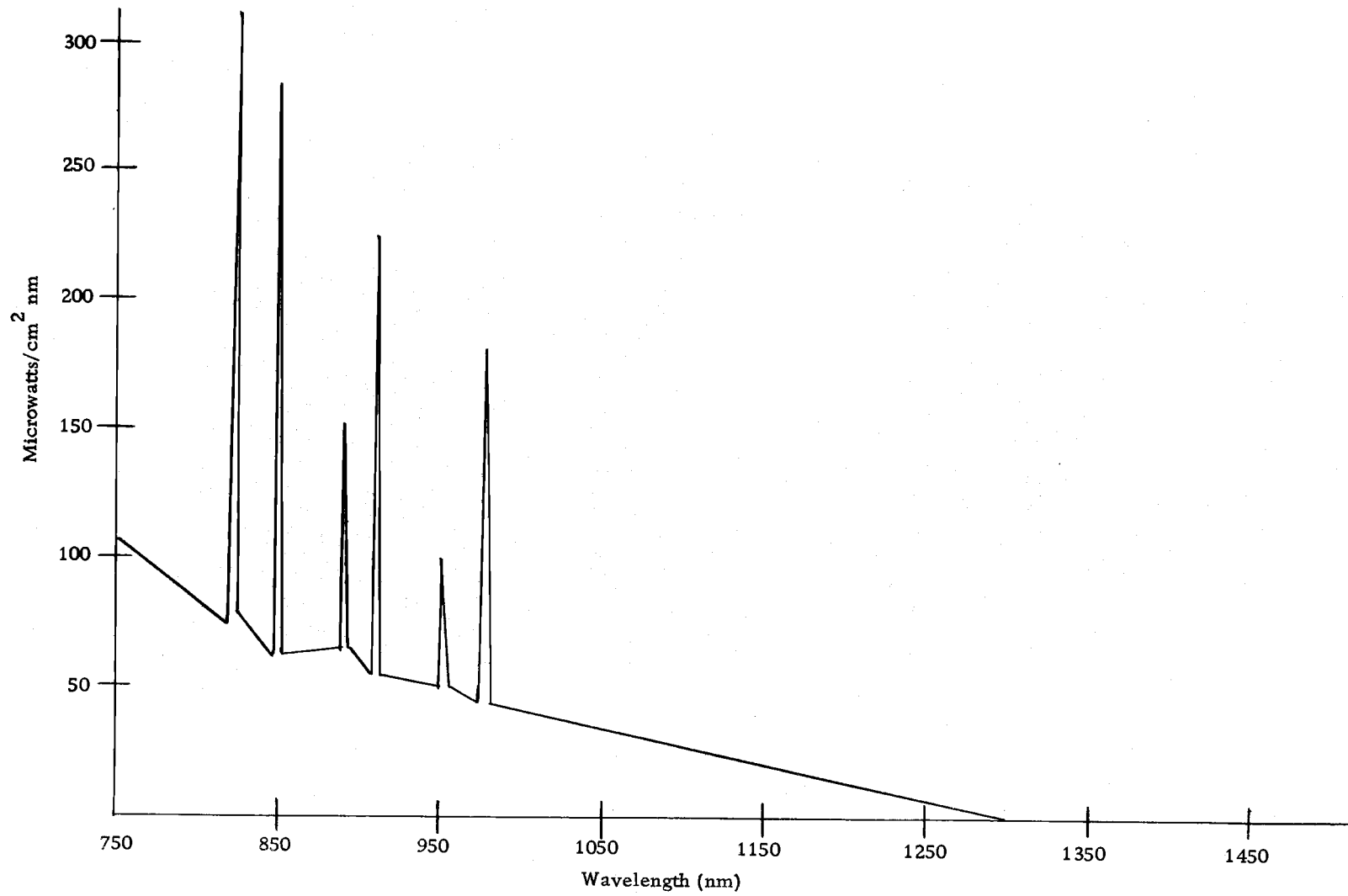


Figure 3B. Infrared spectrum of xenon arc with inner IR filter and outer quartz filter.

which is controlled by a 24-hour time clock. Two additional filters can be manually inserted to give a wide range of light energies. The light energy as a function of filter combinations is presented in Table 6 on page 73 in the Appendix. The spectrum for the xenon arc and for the filtered arc is shown on page 72 in the Appendix.

Temperature Control. Dry bulb temperature is controlled $\pm 0.5^{\circ}\text{C}$ within the range from 4 to 45°C with lights either on or off. The controller is a solid state proportional type that pulses either refrigerant to the cooling coil or current to the 1000 watt heater. Temperature can be adjusted manually by a set point programmer or programmed automatically with a 24-hour cam programmer.

Wet Bulb Depression Control. Wet bulb depression is also programmed with either set point or cam programmer. Humidification is by steam from a distilled-water steam generator and dehumidification is by one of two systems. One system involves vapor diffusion to a cooling coil with a minimum dew point of 7°C with maximum relative humidity (r. h.) approximately 90%. Vapor pressure can be controlled with a maximum transpiration load of 0.4 liters per hour. The other system is a self-generating chemical dehumidification system capable of maintaining a 5% r. h. with a transpiration load of 2.0 liters per hour. Both wet bulb and dry bulb temperatures are monitored on a seven day recorder.

Air Flow. Air circulation horizontal to the plant bed is

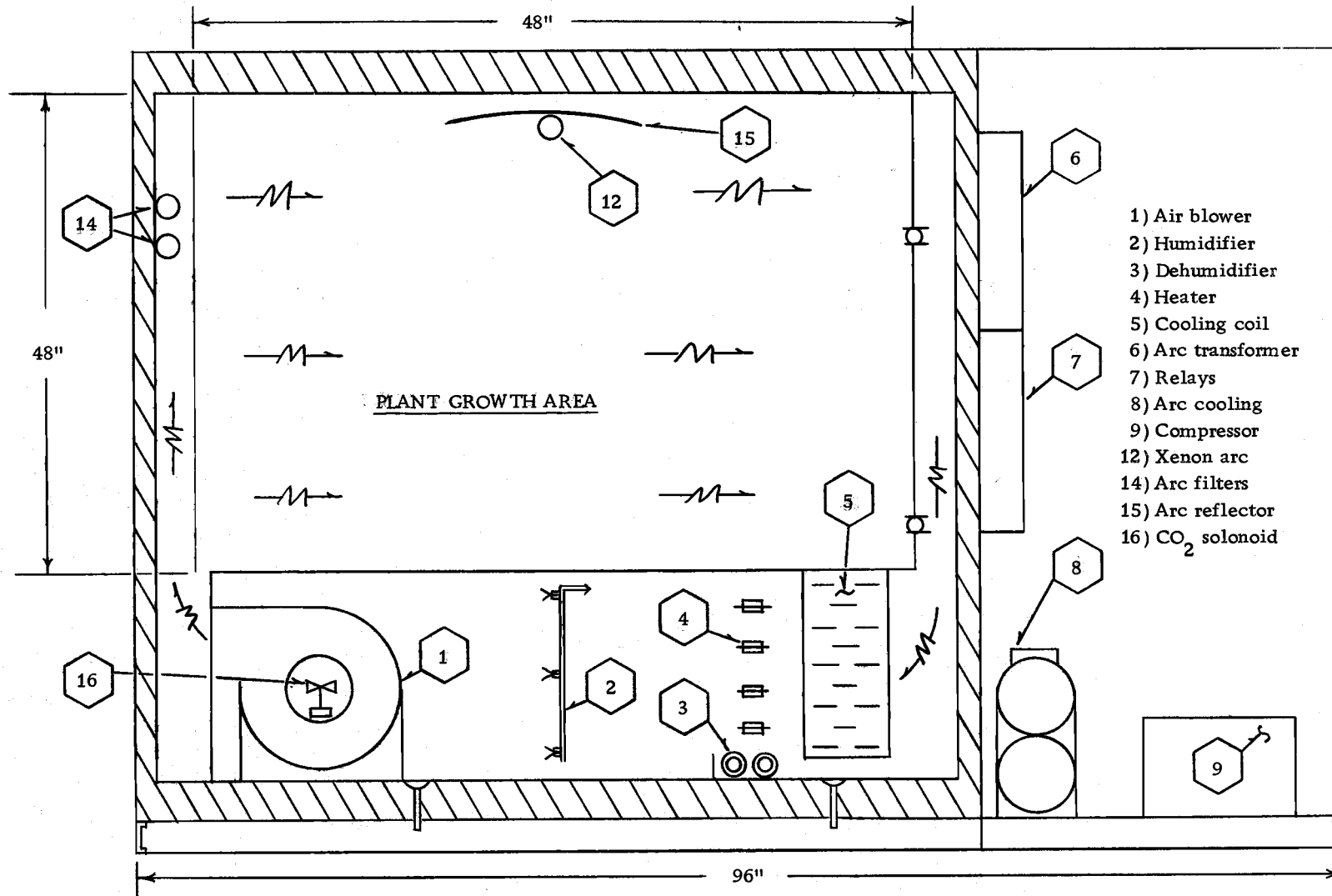


Figure 4. Controlled Environment Chamber, Side View

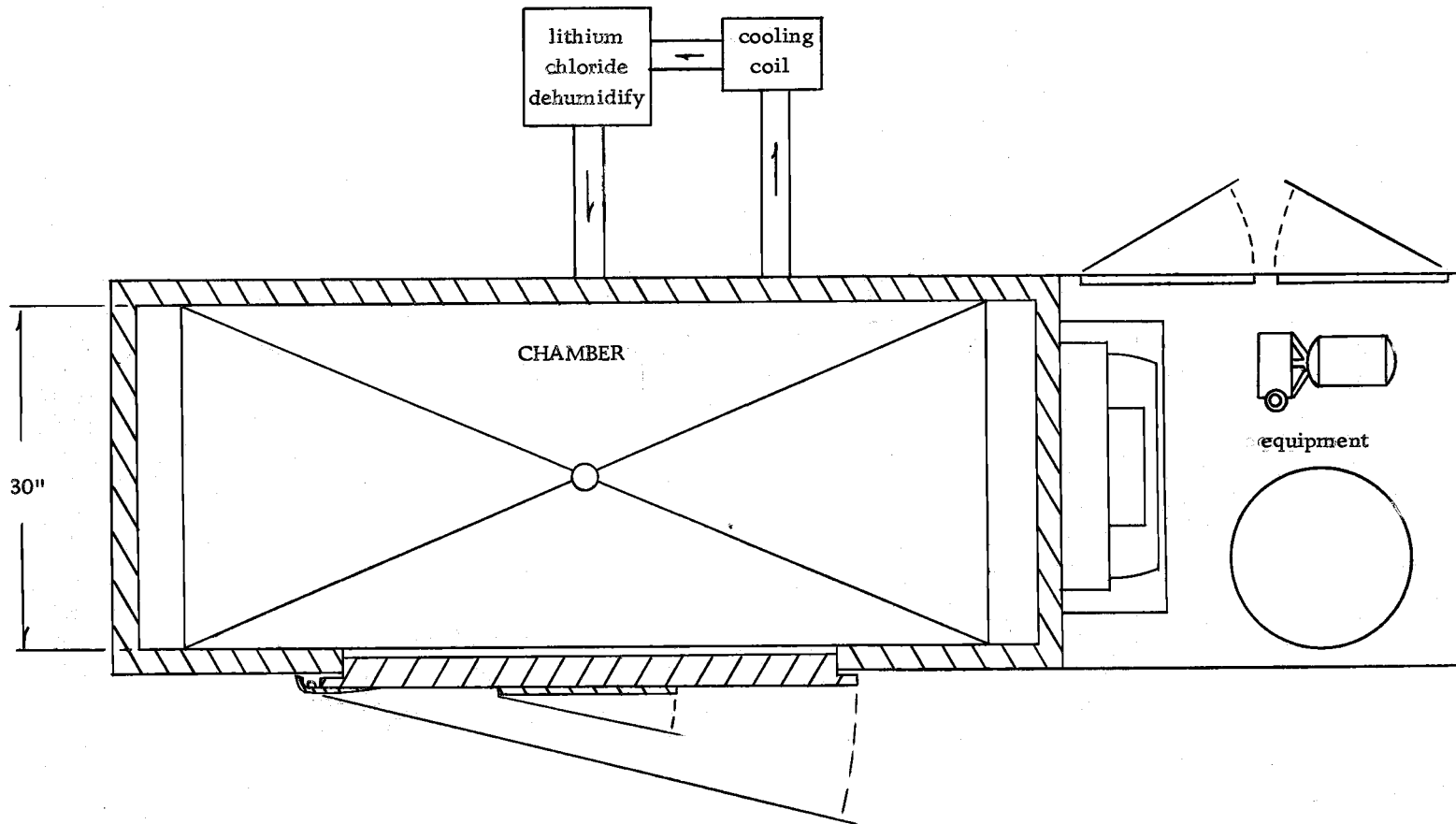


Figure 5. Controlled Environment Chamber with Chemical Dehumidification System. Top View.

approximately 1.5 miles per hour with higher velocities across the lamp and light filters. Both the supply of air to the plant growth area and the return air are channeled through perforated stainless steel at the ends of the chamber to obtain uniform horizontal velocities.

Growth Medium Control

The alder seedlings were grown in a nutrient flow system which is schematically represented in Figure 6. Plants were sealed in five separate 2" i. d. polyvinyl chloride (PVC) tubes with a 3/8" close nipple and automobile distributor wire sealing boot filled with a sealing compound that solidifies by reacting with atmospheric water vapor (see Figure 6). Mercury monometers monitored the pressure in each of the PVC tubes; clamps were used to keep the pressure of each tube at less than 1.2 psi.

Flow rate of the nutrient was maintained at four gallons per minute with a variable flow pump. (All fixtures in the system were either PVC, tygon, or stainless steel.) Aeration was continuous (see Figure 6) and transpired water was replaced with distilled water controlled by a water-level regulator. Temperature was thermostatically regulated with a mercury resistance element located in the manifold and was controlled by water circulating from a water bath through a stainless steel heat exchanger.

Both the variable flow pump and the normally open solenoid on

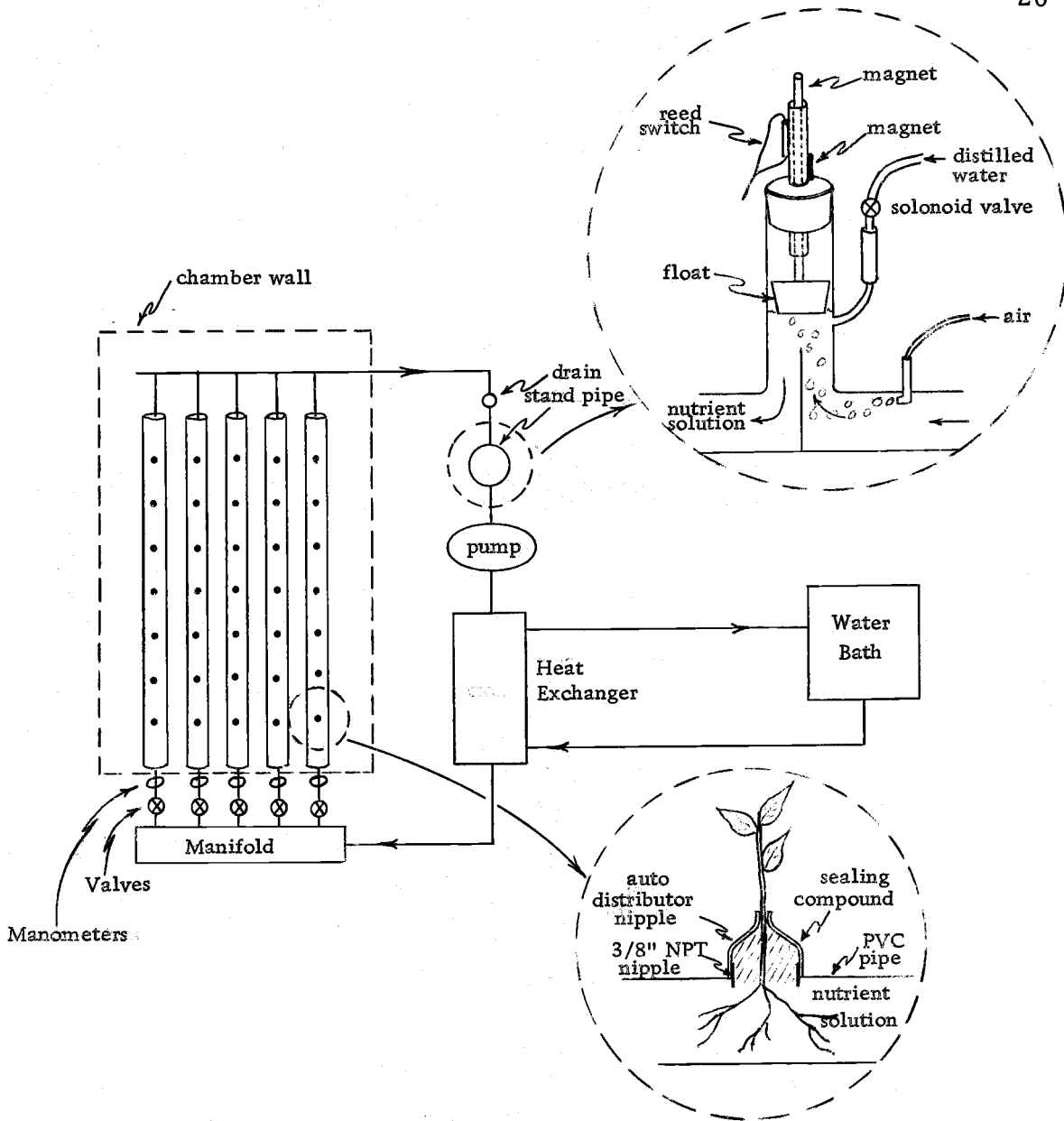


Figure 6. Nutrient Control System

the distilled water line were wired to a double-pole single-throw (DPST) relay that was activated by magnetic closure of the reed switch located at the stand pipe (see Figure 6). If the flow system developed a large leak, the relay closed the solenoid and, simultaneously, shut off the pump.

Carbon Dioxide Control and Measurement

The controls for maintaining CO_2 in the chamber are diagrammed in Figure 8. The CO_2 concentration was monitored continuously during the day by the air flow system external to the chamber. A small magnet, mounted on the recorder arm, closed a hermetically sealed reed switch located on the recorder when the CO_2 concentration in the chamber reached a predetermined level (usually 320 ppm). This activated a variable time delay relay which opened a normally closed solenoid located inside the blower in the chamber and a short burst (two to five seconds) of CO_2 entered the chamber from a pressurized bottle. The burst of CO_2 was precalibrated to raise the CO_2 concentration in the chamber back to the desired level (normally 335 ppm). Distribution of CO_2 in the chamber took about ten seconds.

The CO_2 measuring system is a semi-open system similar to many used by other workers. The system is diagrammed in Figure 8. Air is sampled at the base of the supply-air plenum in the chamber and driven through the tygon system at the rate of 0.7 liters per

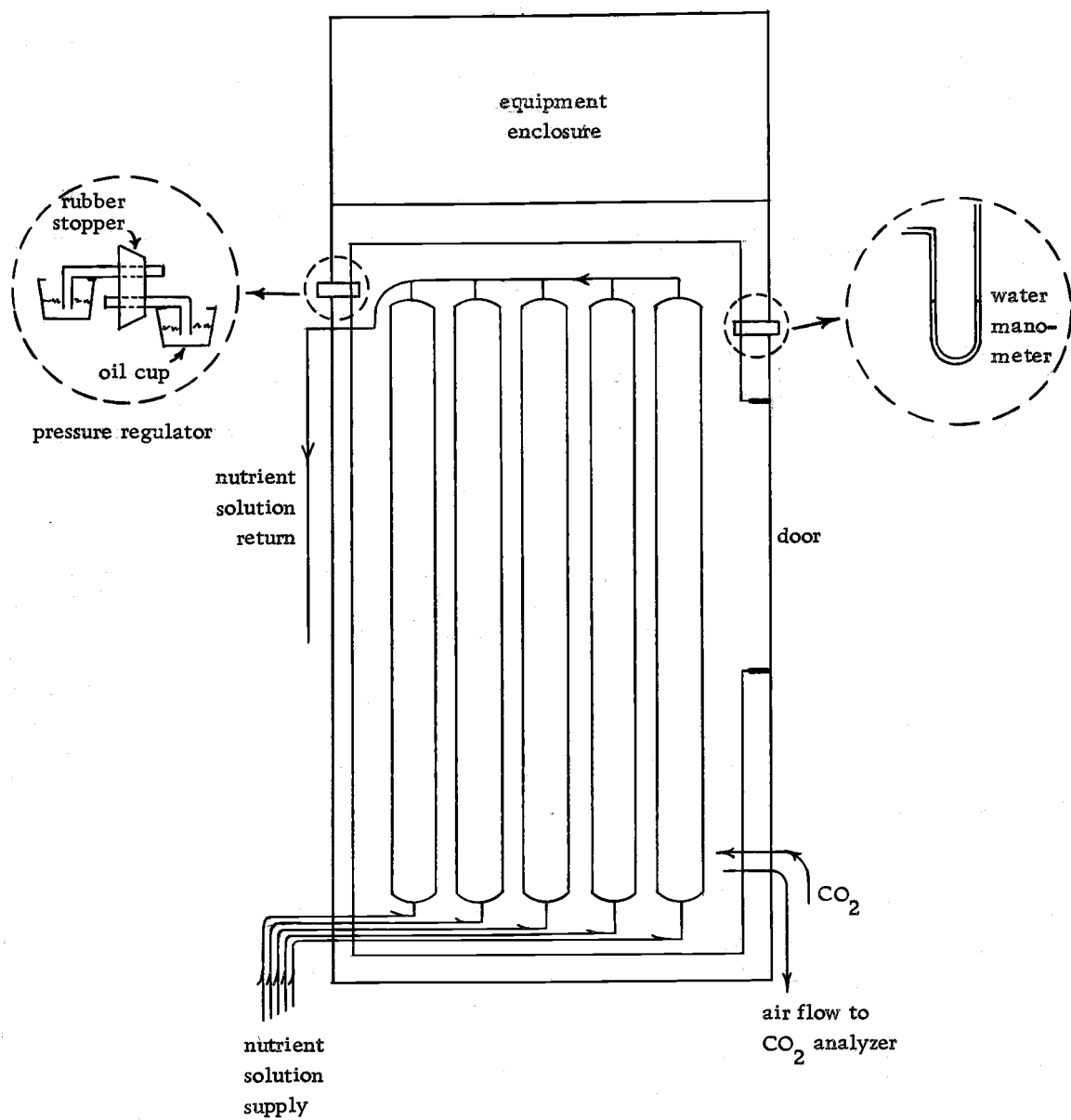


Figure 7. Environment Chamber Accessories

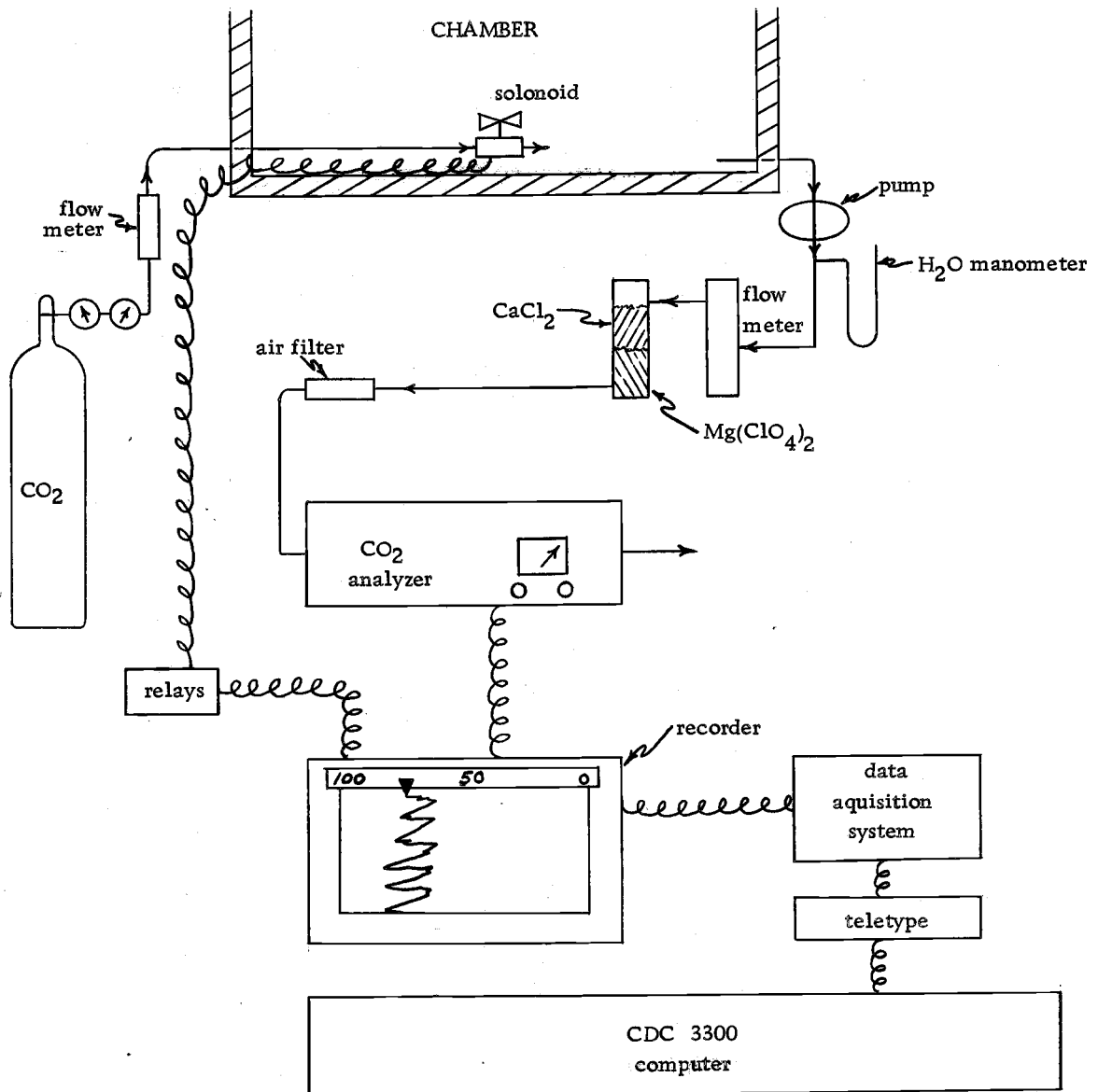


Figure 8. CO₂ Measuring & Control System

minute with a peristaltic pump. Water vapor is removed from the air sample with eight-mesh calcium chloride and magnesium perchlorate. The air is exhausted to the atmosphere after passing through the gas analyzer.

Plant Community and Environmental Program

After an initial experiment to determine the reliability of the system, a second experiment determined photosynthetic response of a small red alder community to light and temperature at steady-state conditions. These data were modeled with a multiple linear regression technique and a non-linear structural model prior to a third experiment testing the prediction power of the regression model under dynamic conditions of light and temperature.

One-year-old alder seedlings, 6 to 12 inches tall, were removed in February, 1970 from a site in the Coast Range 20 miles east of the Pacific and stored in a cold room before transplanting to the greenhouse. Plants were grown in an aerated nutrient solution (see Appendix, p. 78) which was changed weekly. Day length in the greenhouse was maintained at 14 hours with a single bank of cool white fluorescents augmented with incandescent bulbs. Total short-wave radiation from the artificial lights was 0.021 ly/minute. Light energy in the greenhouse during daylight hours ranged from 0.042 ly/minute under cloudy conditions to 0.14 ly/min under full sunlight.

Day temperature was 21°C, and night temperature was 10°C.

Experiment One

After several weeks in the greenhouse, the seedlings were transplanted to PVC tubes, and placed in the environment chamber three days later. The chamber was programmed with the following environmental conditions for one month prior to photosynthetic measurements: Light energy was changed in a stepwise fashion at two-hour intervals using the retractable filters to simulate the increasing and decreasing radiation of a fully sunlit day (see Figure 9). Dry bulb temperature and wet bulb depression were programmed as a sine function, with a minimum of 11°C at 3 AM and a maximum of 26°C at 3 PM (see Figures 34 and 35 in Appendix).

Qualitative information on morphological response of alder growing under xenon light was noted. The photosynthetic light saturation curve for this community was determined as follows: Photosynthetic rates were measured in duplicate between 320 and 350 ppm ambient CO₂ at five light energies. The light sequence was programmed from low to high with a 20 minute interval for plant equilibrium between measurements.

Experiment Two

In the second experiment, plants were grown in the greenhouse

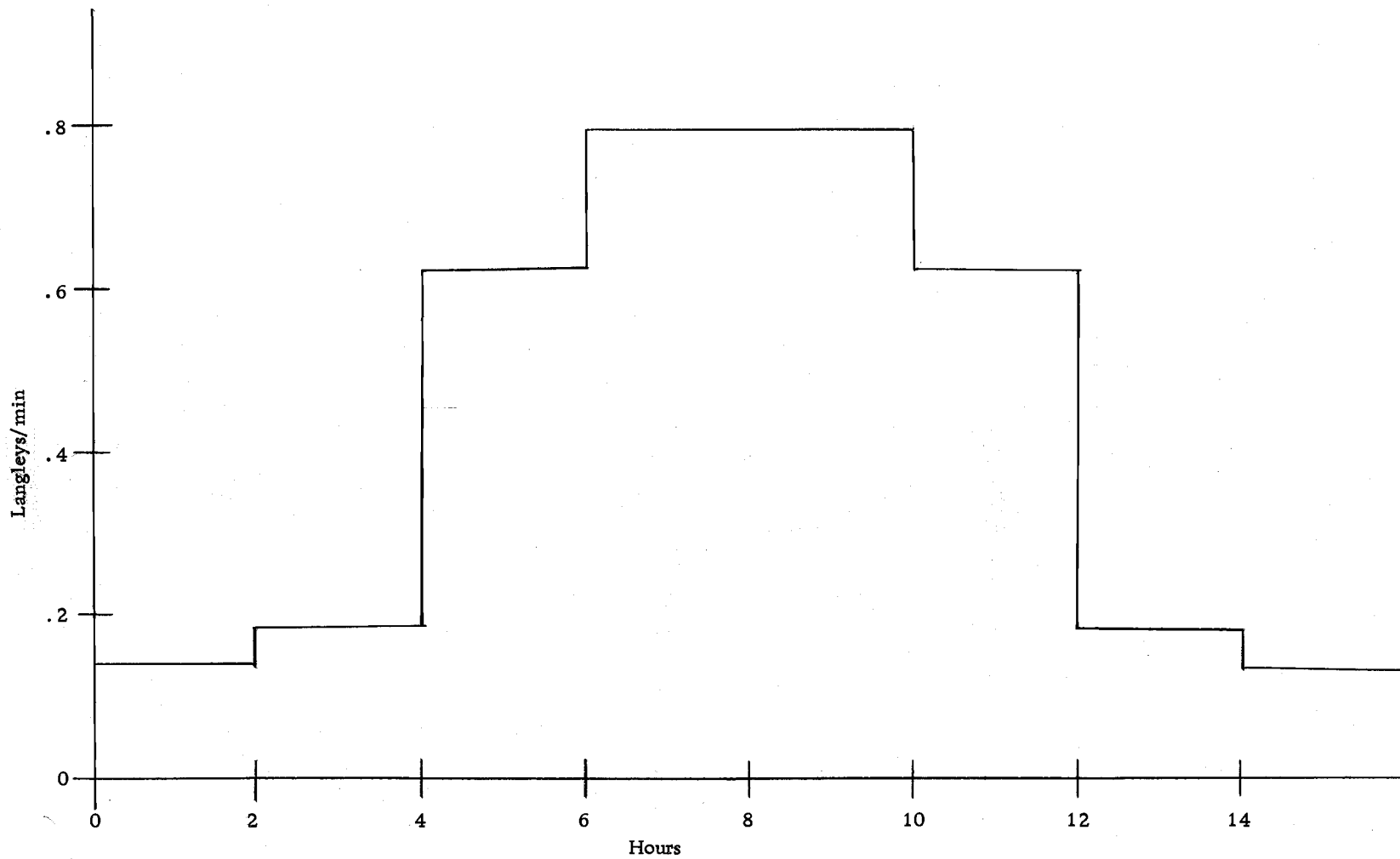


Figure 9. Daily short-wave radiation pattern of alder community, experiment 1.

under the above environmental conditions and transplanted to PVC tubes four weeks before being placed in the chamber. The plants were maintained under environmental conditions consistent with those in the greenhouse for one week prior to taking steady-state photosynthetic data.

Net photosynthesis was measured as a function of light energy and dry bulb temperature within a range of 0.06 to 0.68 ly/minute (total short-wave radiation) and 5 to 30°C dry bulb temperature. For each of five light levels, dry bulb temperature was changed at the rate of 1° per five minutes, beginning at 15°C and proceeding upscale to approximately 30°C. Measurements were then made by decreasing temperature at the same rate until near 5°C at which time temperature was increased again until 16°C. All measurements were made during three successive days. Root temperature was held at 12°C ± 1°C and wet bulb depression was held at 4°C ± .75°C.

Environmental variables were monitored at the plant level in the chamber at one minute intervals throughout the experiment. Radiation was monitored with a Kipp solarimeter located in the center of the chamber near the top of the plants. Wet bulb depression and dry bulb temperature were monitored with an electric psychrometer from air sampled from the center of the plant community. Root temperature was monitored with a thermocouple located in the center PVC tube. All data were digitized onto paper tape with a 25-channel

data acquisition system and relayed to the computer from a laboratory teletype. Photosynthetic measurements were made between 320 and 335 ppm CO₂ from data taken from the strip-chart recorder.

Experiment Three

Non steady-state photosynthetic data were taken on the same plants for a 14-hour day for the purpose of comparing photosynthetic measurements to those predicted from an equation developed from steady-state data. Root temperature and wet bulb depression were held constant as in Experiment Two. Temperature was varied according to the pattern in Figure 10 and light energy was changed in a step function to simulate sunrise and various cloud conditions (see Figure 11). Data were recorded at one to two minute intervals over a three day period.

The steady-state predictive equation was determined using a stepwise multiple linear regression routine. Structural analysis of the data was obtained with a non-linear curvefit program.

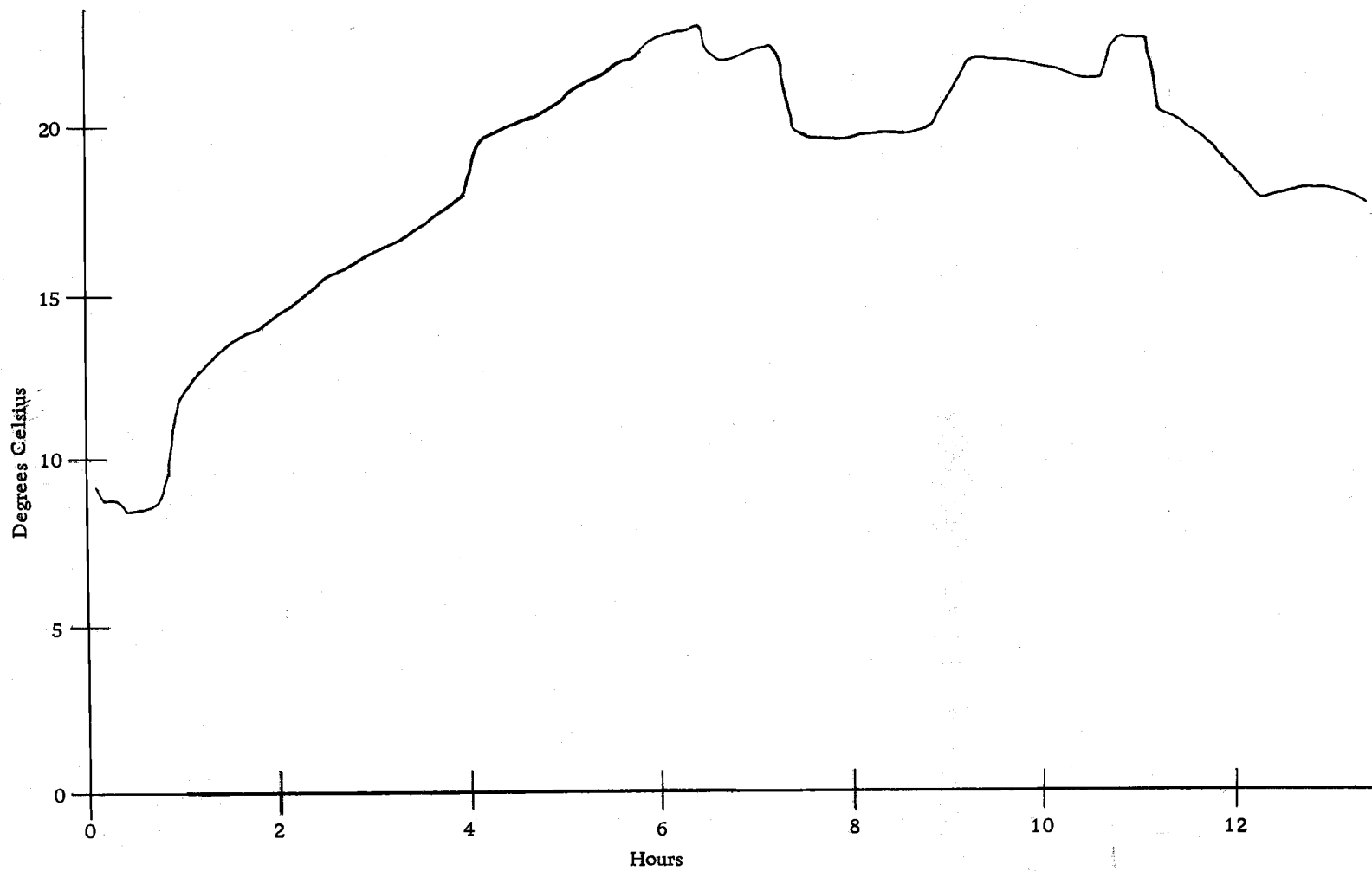


Figure 10. Temperature time curve for experiment 3.

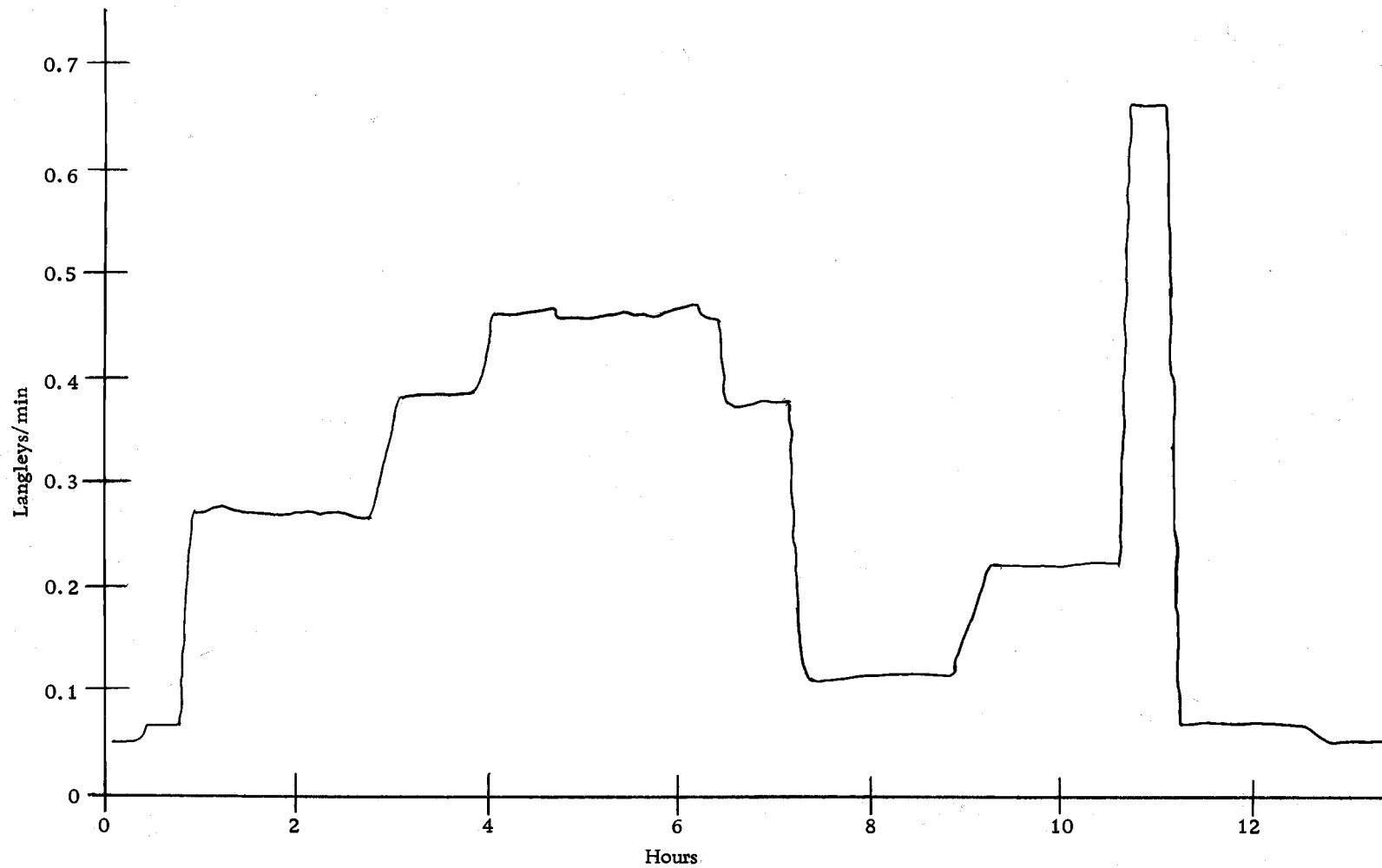


Figure 11. Radiation time course for experiment 3.

RESULTS AND DISCUSSION

General morphological differences between alder seedlings grown in the greenhouse and those raised under xenon light were striking. The leaves of the greenhouse plant were large (up to 18 cm long) and dark green while those grown under xenon were much smaller (less than 8 cm long), were light green, and had a slightly cupped appearance. Petioles of greenhouse-grown plants had a slight red tinge while those grown under xenon were several shades brighter. At maximum light intensities, some injury of the leaves was noticed when leaves of adjacent plants rubbed against one another.

Experiment One

Carbon dioxide exchange in response to increasing light intensity was observed in Experiment One (Figure 12) where plants were preconditioned for one month under a total daily short-wave radiation of 670 langleys. The shape of the curve is similar to that for individual plants except that photosynthesis is not clearly saturated at high light energies. (There are too few data points to use a general curve-fit routine to verify the presence or absence of light saturation.) The absence of the saturation phenomenon for plant communities has been predicted by many other workers (Gaastrri, 1963; Kramer and Kozlowski, 1960). The maximum net photosynthetic rate of 12 mg CO₂/gm leaf dry weight/hour is lower than found by Krueger and

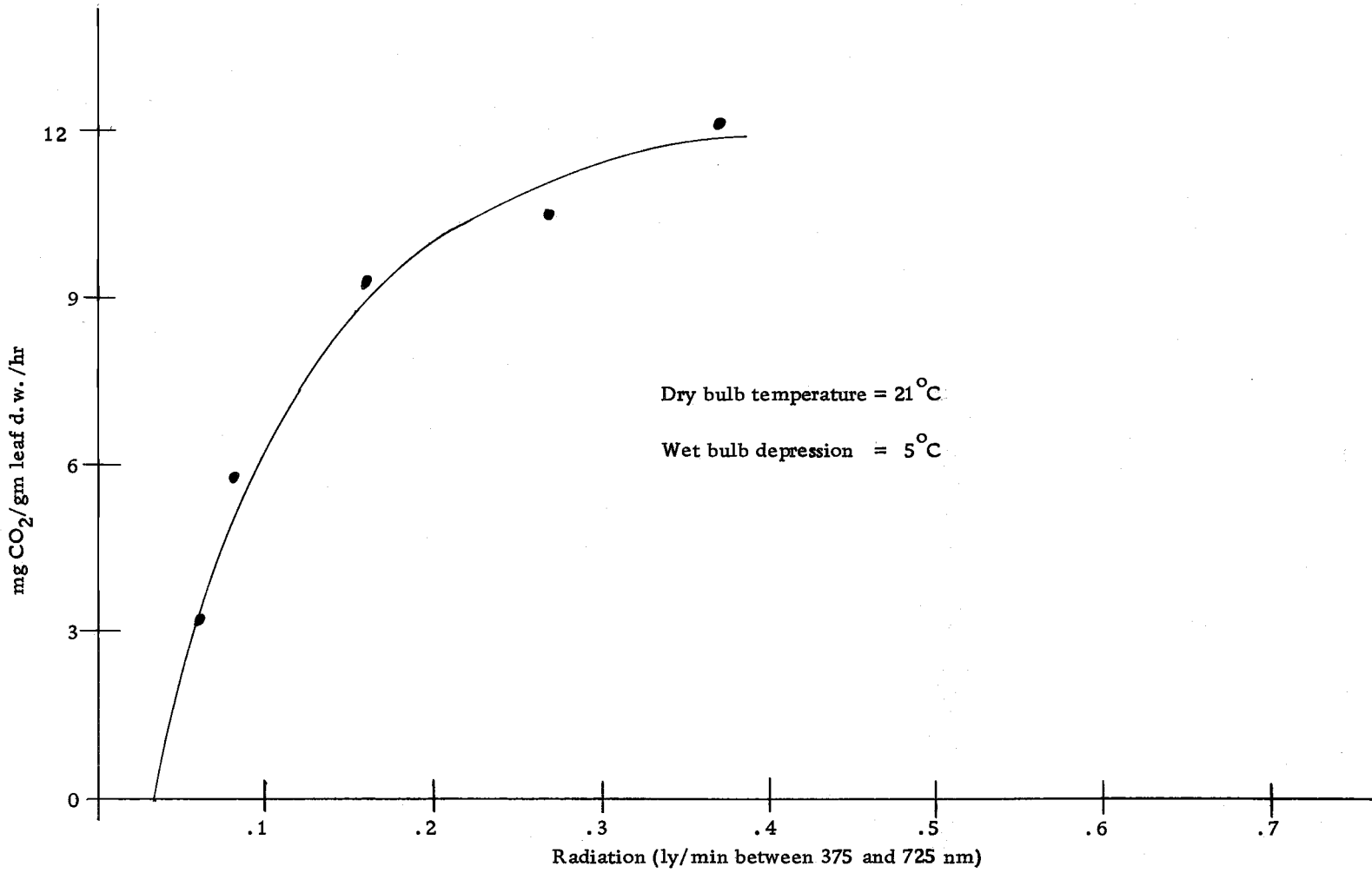


Figure 12. Light curve for red alder community. Experiment 1.

Ruth (1969). They found that the photosynthetic rates for single leaves of alder plants preconditioned in 70% full sunlight photosynthesized at 30 mg/gm/hr in the saturated region of the light curve. The apparent low photosynthetic rates may reflect some chlorophyll destruction resulting from a month of radiation levels that were considerably higher than those in the greenhouse where the plants were preconditioned. More likely, the lower rates reported here result from self-shading within the alder community.

Experiment Two

Stepwise Multiple Linear Regression Models

The steady-state photosynthetic data from Experiment Two was analyzed with a linear stepwise multiple regression routine to establish a predictive equation and to determine the relative contribution of each variable in explaining the environmentally controlled variation in net photosynthesis. Although radiation and temperature are the two major variables, the small uncontrollable variation in root temperature ($\pm 1^{\circ}$), and vapor pressure deficit (± 1.0 mb) was included to determine if this minor variation contributed significantly to the variation in net photosynthesis.

The result of the first stepwise analysis is summarized in Table 1. The F-level to enter a variable and to remove a variable was set at 2.0. Radiation was transformed to a logarithmic function

Table 1. Summary of first stepwise analysis.*

| Variable | Units | Coefficient | F-level | R ² |
|-------------------------|--------|-------------|---------|----------------|
| Constant | | 111.9 | | |
| log ₁₀ (rad) | ly/min | 54.2 | 374 | .66 |
| air T | °C | 6.7 | 140 | .81 |
| v. p. d. ** | mb | 26.4 | 22 | .83 |
| (air T) ³ | °C | - .003 | 12 | .84 |

* 189 observations

** vapor pressure deficit

$$P_{sn} = 111.9 + 54.2 \log X_{rad} + 6.7X_{air T} - .0033X_{air T}^3 + 26.9X_{vpd} \quad (1)$$

and air temperature was both squared and cubed. Radiation and the linear component of air temperature account for 81% of the total variation in net photosynthesis, with F-levels of 374 and 140, respectively. Vapor pressure deficit and the cubic air temperature function account for the remaining 3% of variation and both have significant F statistics at the 5% level. Both root temperature and quadratic function of air temperature failed to meet the F-level criteria of 2.0 and were dropped from the analysis.

Table 2 summarizes a stepwise analysis in which radiation was fitted to a cubic polynomial, the air temperature squared term was dropped, and the F-level criteria for entering or removing the variable was set at zero.

Table 2. Summary of second stepwise analysis.

| Variable | Coefficient | F-level | R ² |
|----------------------|-------------|---------|----------------|
| Constant | - 57.5 | | |
| rad | 1127.1 | 165.8 | .47 |
| (rad) ² | -1972.5 | 159.4 | .71 |
| air T | 7.2 | 170.4 | .85 |
| (air T) ³ | - .0035 | 31.5 | .87 |
| (rad) ³ | 1072. | 17.7 | .88 |
| vpd | 17.9 | 11.0 | .89 |
| root T | - 4.2 | 2.5 | .89 |

$$\begin{aligned}
 P_{sn} = & -57.5 + 1127.1X_{rad} - 1972.5X_{rad}^2 + 1072X_{rad}^3 + \\
 & 7.24X_{air\ T} - .0035X_{air\ T}^3 + 17.9X_{vpd} - \\
 & 4.2X_{root\ T}
 \end{aligned}
 \tag{2}$$

The above regression equation explains 89% of the photosynthetic variation, 88% of which is explained by air temperature and radiation terms. The algebraic sign of the radiation and temperature coefficients are generally those expected; however, the positive coefficient for the radiation cubed term would indicate a continually increasing photosynthesis at high light energies which is contrary to the expected light saturation phenomena. The positive sign probably represents an artifact resulting from a lack of data between 0.25 ly/minute and 0.68 ly/minute which causes the coefficient of the cubic term to go positive to minimize the squared deviations. This

examplifies the danger in extrapolation of polynomial models without some prior knowledge of the physical constraints on the system.

The F-level of 2.5 for root temperature is not significant at the 5% level for 1 and 180 degrees of freedom. The F-level for the vapor pressure deficit term is 11.0 which is significant at the 5% level. However, this term increases the total r^2 term by only .007.

Table 3 summarizes the results of another stepwise analysis in which vapor pressure deficit and root temperature were dropped from the analysis and two interaction terms between radiation and air temperature were included. The F-level for entering or excluding a variable was set at zero.

Table 3. Summary of third stepwise analysis.

| Variable | Coefficient | F-level | R ² |
|--------------------------|-------------|---------|----------------|
| Constant | 63.8 | | |
| rad · air T | 74.1 | 288.1 | .60 |
| rad ² · air T | - 76.1 | 160.9 | .79 |
| (air T) ³ | - .0099 | 506.4 | .94 |
| air T | 1.001 | 20.3 | .95 |
| rad | 357.9 | .09 | .95 |
| (rad) ³ | 1821.4 | 28.1 | .96 |
| (rad) ² | -1783.1 | 138.6 | .98 |

$$\begin{aligned}
 P_{sn} = & 63.8 + 357.9X_{rad} - 1783.1X_{rad}^2 + 1821.4X_{rad}^3 + \\
 & 1.001X_{air\ T} - .0099X_{air\ T}^3 + 74.1X_{rad} \cdot X_{air\ T} - \\
 & 76.1X_{rad}^2 \cdot X_{air\ T}
 \end{aligned} \tag{3}$$

All variables in this predictive equation are highly significant according to the F-level criteria except for the linear radiation term. Evidently, most of the variation due to this term has been explained in the two interaction terms, radiation times air temperature and radiation squared times air temperature. Inclusion of these multiplicative interaction terms has increased the explained variation to 98% from 89% in the previous stepwise analysis (see Table 2). The signs of the coefficients are consistent with the physical system. This predictive regression equation accounts for 98% of the total variation in net photosynthesis but is only reliable for this plant system under the experimental environmental conditions.

Non-linear Structural Response Model

An alternative to the previous additive response model is a non-linear model whose coefficients have a theoretical basis. Such models are conceptually more reliable, and extrapolation to other systems can be accomplished with more confidence.

A photosynthetic response model can best be structured around the light saturation curve which, under optimum environmental conditions, determines the maximum net gain in productivity.

The mathematical formulation of the curve shown in Figure 13 can take several different forms. One form is the expression:

$$Z = B_0 + B_1(1 - e^{-B_2 Y}) + B_3 Y \quad (4)$$

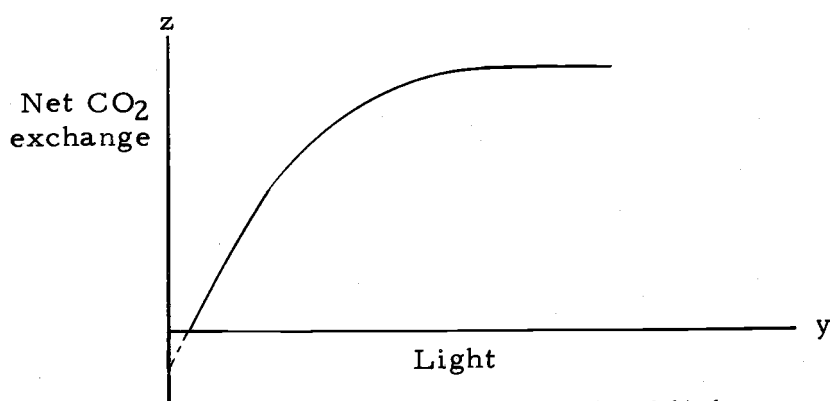


Figure 13. Generalized light curve.

where

Z = net photosynthesis (Psn); either relative or absolute units

Y = radiation in ly/minute

The coefficients relate to the following physiological responses:

B_0 = respiration; Z intercept when radiation is zero

B_1 = maximum net photosynthesis for a given temperature

B_2 = transition region, approaches linearity for low radiation

B_3 = slope of asymptote that Psn approaches at high radiation

Both B_0 and B_2 have negative signs while B_1 is positive. B_3 can be zero, negative, or positive, depending upon whether the response approaches a zero derivative asymptote as for a single leaf, whether the response is negative as in chlorophyll destruction, or whether the response is positive as in heavy self-shading within a plant community. (In the latter case the coefficient, B_3 , would probably be a function of the leaf area index (LAI).) B_0 and B_1 (respiration and maximum net photosynthesis) are both dependent on temperature, but B_2 and B_3 are temperature independent. Expression (4) can now be

written:

$$Z = f(X) + g(X)(1 - e^{-B_2 Y}) + B_3 Y \quad (5)$$

where

X = temperature in degrees Celsius

$f(X)$ = respiration as function of temperature

$g(X)$ = net photosynthesis as function of temperature

A net photosynthetic response to temperature has been generalized by Pisek (1969) following his comparisons on a variety of plants.

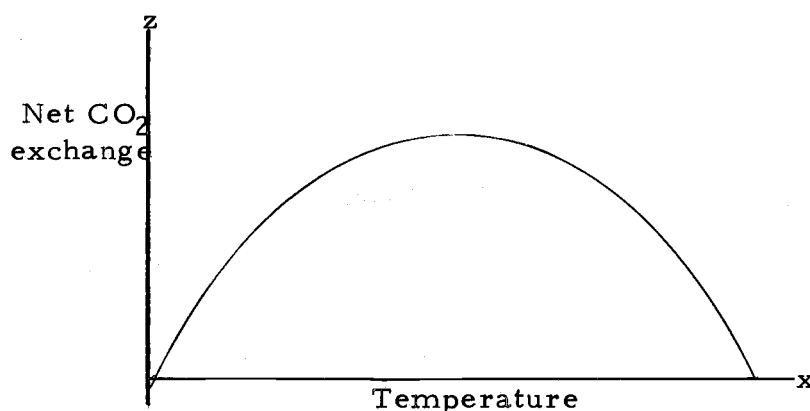


Figure 14. Generalized Psn response to temperature.

This function can be fit by a symmetric quadratic of the following form:

$$g(X) = B_0' + B_1'(X - B_2')^2 \quad (6)$$

This quadratic function is symmetric about B_2' which is the temperature at which photosynthesis has a maximum value of B_0' . B_1' determines the rate of change of photosynthesis with respect to temperature and has units of ppm CO_2 /hr/deg.

The steady-state photosynthetic data is plotted as a function of temperature at each of five radiation levels (see Figure 15). A non-linear curvefit program that uses a least-squares fit criterion was used to estimate the parameters for $g(X)$ at each radiation level. The parameters appear in functional form on Figure 15 and are summarized in the following table.

Table 4. Parameters from Equation (6) for five radiation levels.

| Short-wave radiation (ly/min) | Parameter | | |
|----------------------------------|------------------------------|------------------------------------|------------------------------------|
| | Maximum Psn (B_0') | Slope coefficient (B_1') | Temp. of max. Psn (B_2') |
| .068 | 70.9 | -.35 | 11.8 |
| .150 | 167.4 | -.48 | 19.3 |
| .190 | 196.6 | -.52 | 20.5 |
| .260 | 224.1 | -.57 | 21.1 |
| .680 | 255.5 | -.55 | 23.8 |

If the functional relationship for predicting net photosynthesis from light and temperature is multiplicative (i. e., $g(X)(1 - e^{-B_2 Y})$), each parameter from Table 4 expressed as a function of radiation would be of a form similar to the light curve. Figures 16, 17, and 18 show that these three parameters, expressed as functions of radiation, do closely approximate the light curve form indicating the functional relationship to be multiplicative.

The modeling of respiration (i. e., $f(X)$) over a wide temperature range is more difficult since response functions do not seem

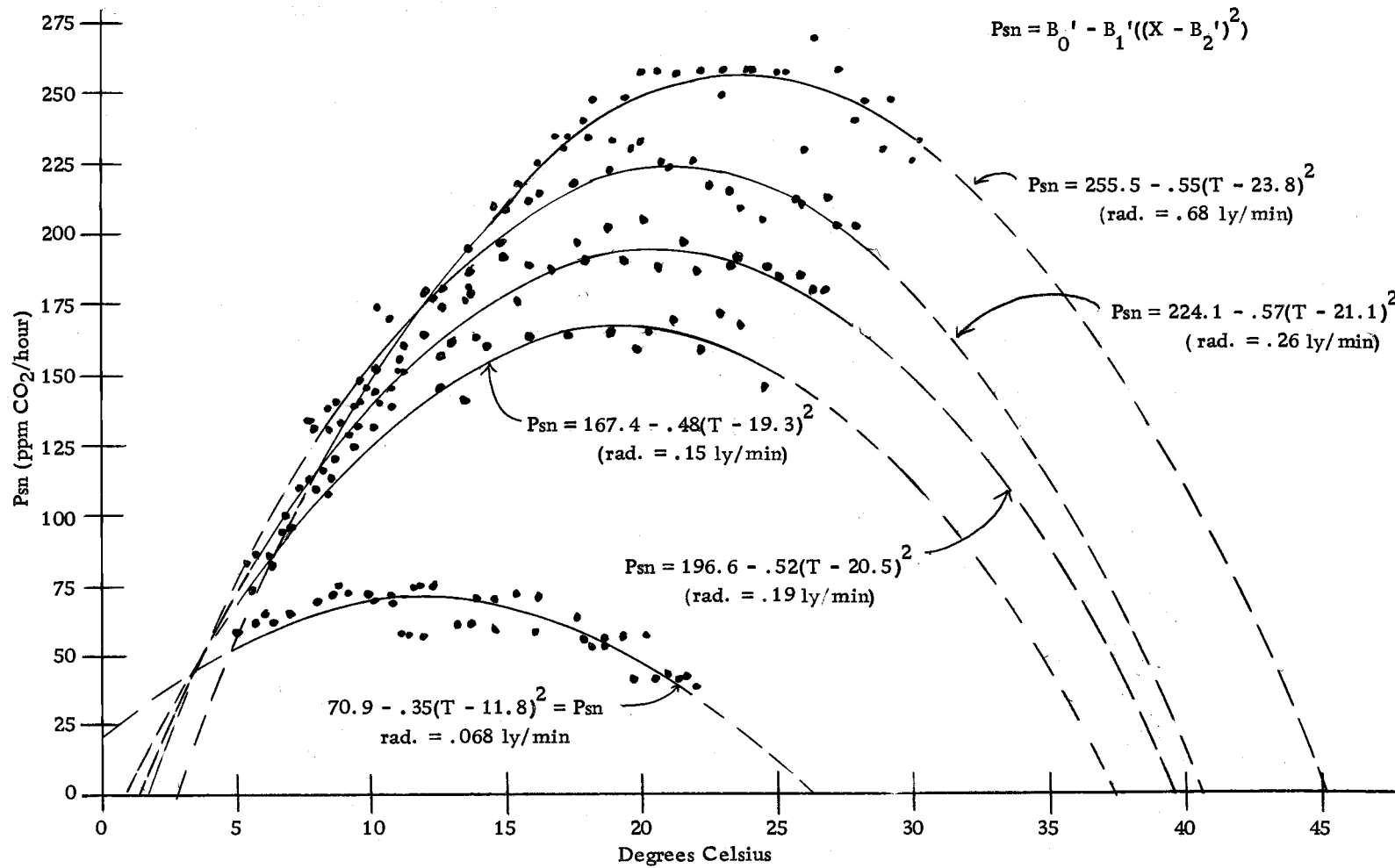


Figure 15. Net photosynthetic response to temperature of five radiation levels. Least-squares curvefit to symmetrical quadratic function.

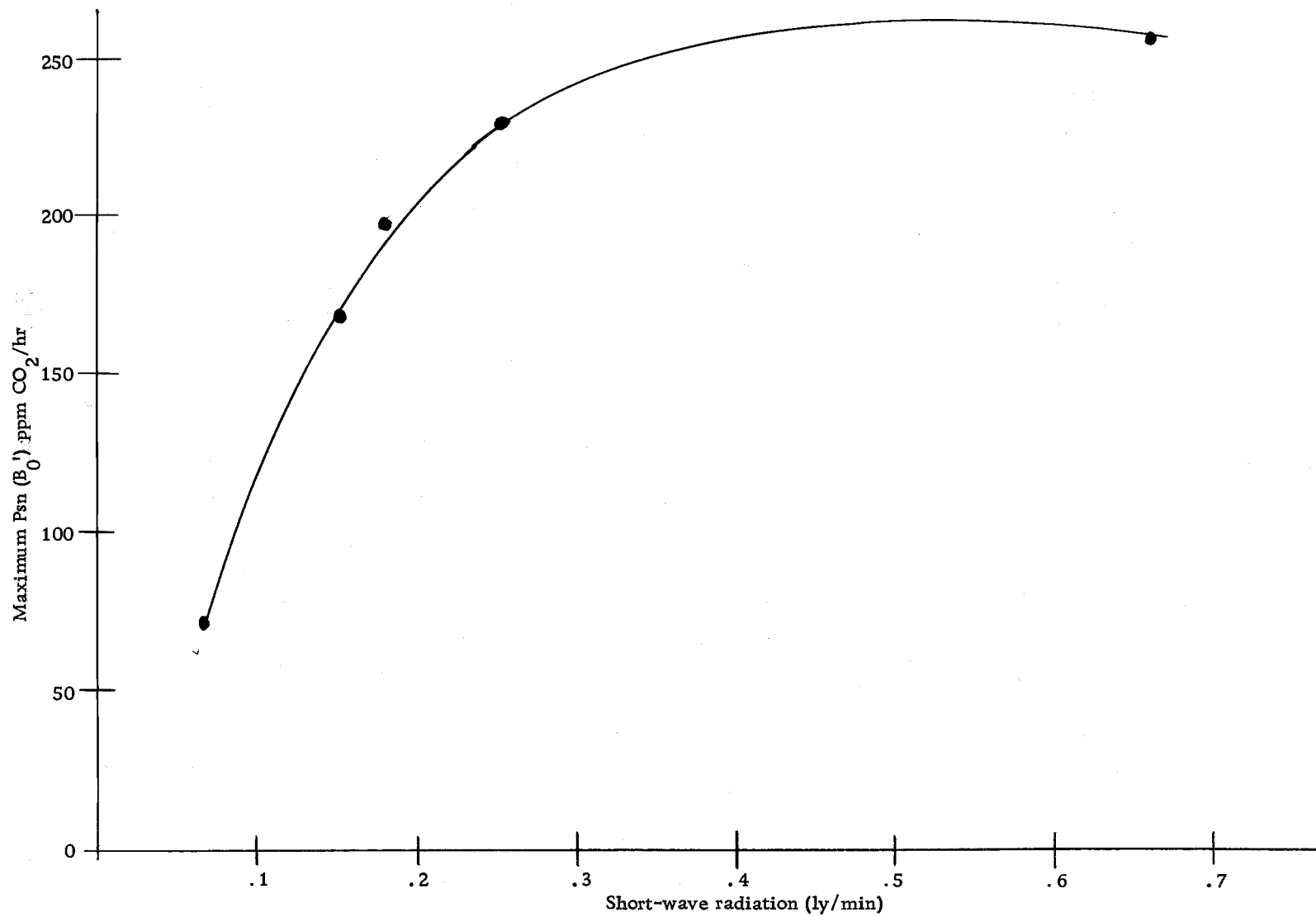


Figure 16. Maximum photosynthetic response to temperature at five light levels.

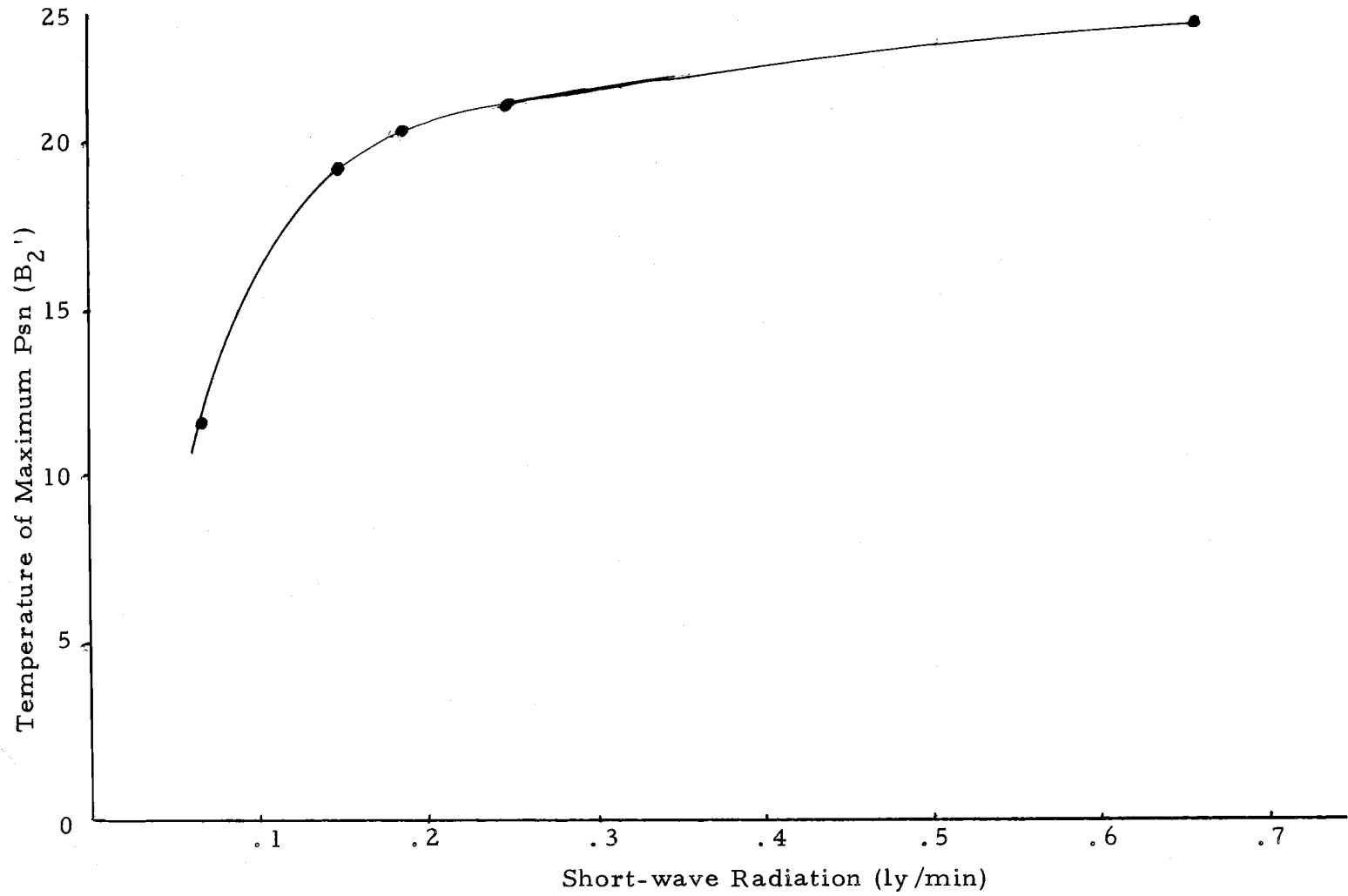


Figure 17. Temperature of maximum photosynthetic response for five light levels.

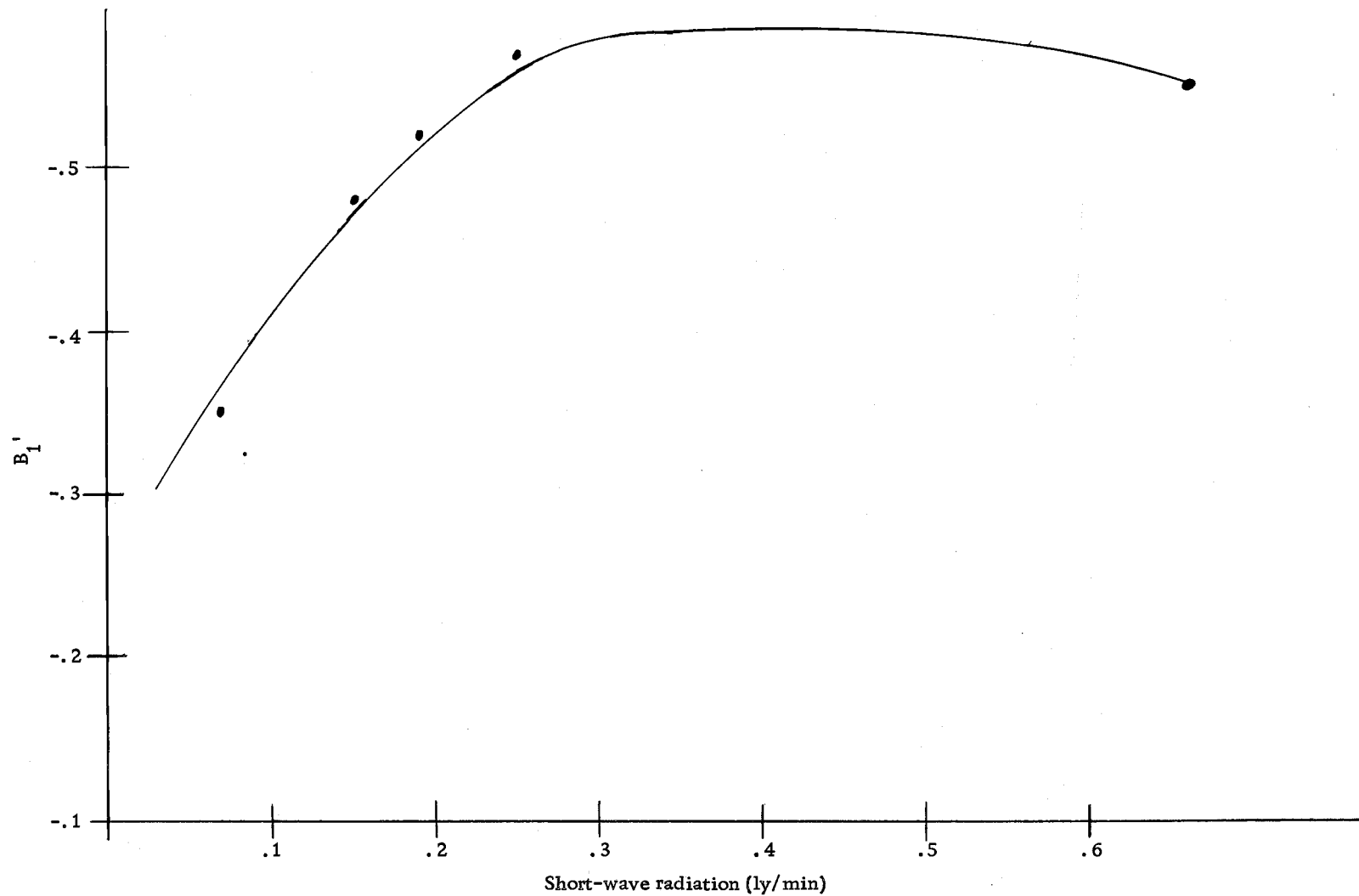


Figure 18. Slope coefficient (B_1') from temperature response equation 3 for five light levels.

readily available from the literature. Also, respiration rates are determined indirectly in this experiment by extrapolation of the photosynthetic light curve to zero and are more subject to error than direct measures.

An estimate of respiration was made by extrapolation of hand-fitted light curves at four temperatures. This data is graphed in Figure 19. Since the relationship is only slightly quadratic, a quadratic and a linear function were used to approximate respiration. A non-linear curvefit technique using a least-squares fit criterion was used to fit the data to the following model:

$$Z = B_0X + (B_1 + B_2(X-B_3)^2)(1-e^{B_4Y}) + B_5Y \quad (7)$$

where

$$B_0X = \text{respiration function} = f(X)$$

$$B_1 + B_2(X-B_3)^2 = \text{Psn temperature function} = g(X)$$

$$(1-e^{B_4Y}) + B_5Y = \text{Light curve function}$$

Figures 20 and 21 illustrate three viewpoints for the surface generated by the function:

$$Z = -5X + (391.3 - .457((X-28.98)^2))(1-e^{-10.05Y}) + .0012Y \quad (8)$$

Inspection of the response surfaces indicates that, generally, the functions represent the expected Psn response of the plant system. The single inaccuracy is the predicted increase in Psn at zero light for negative temperatures. This is probably an artifact of the function

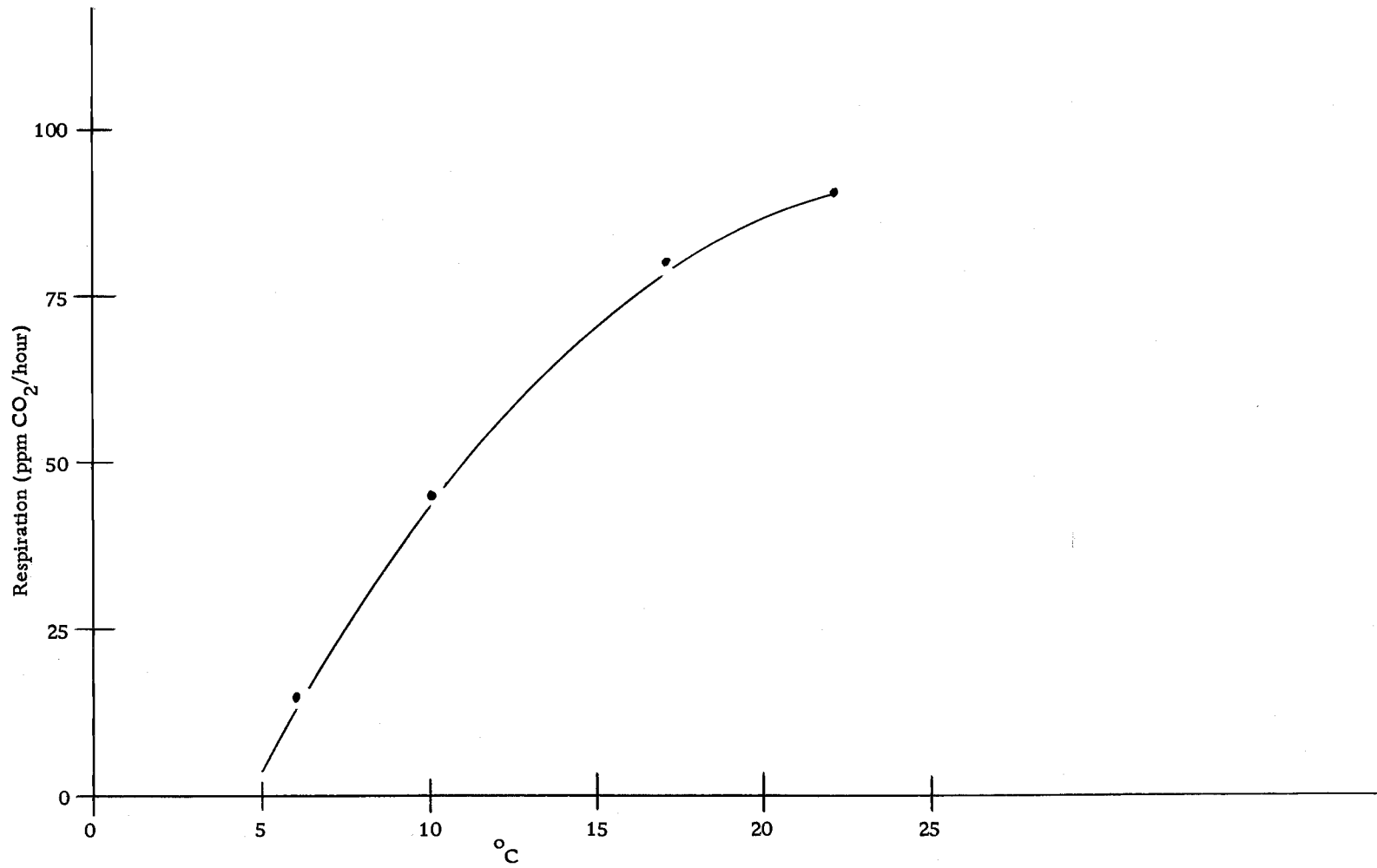
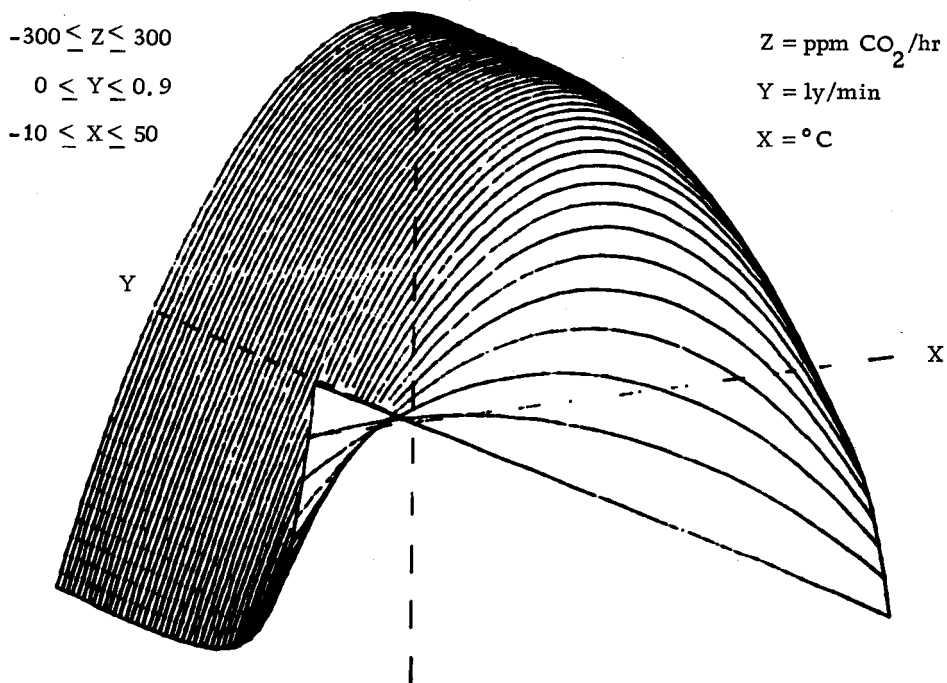


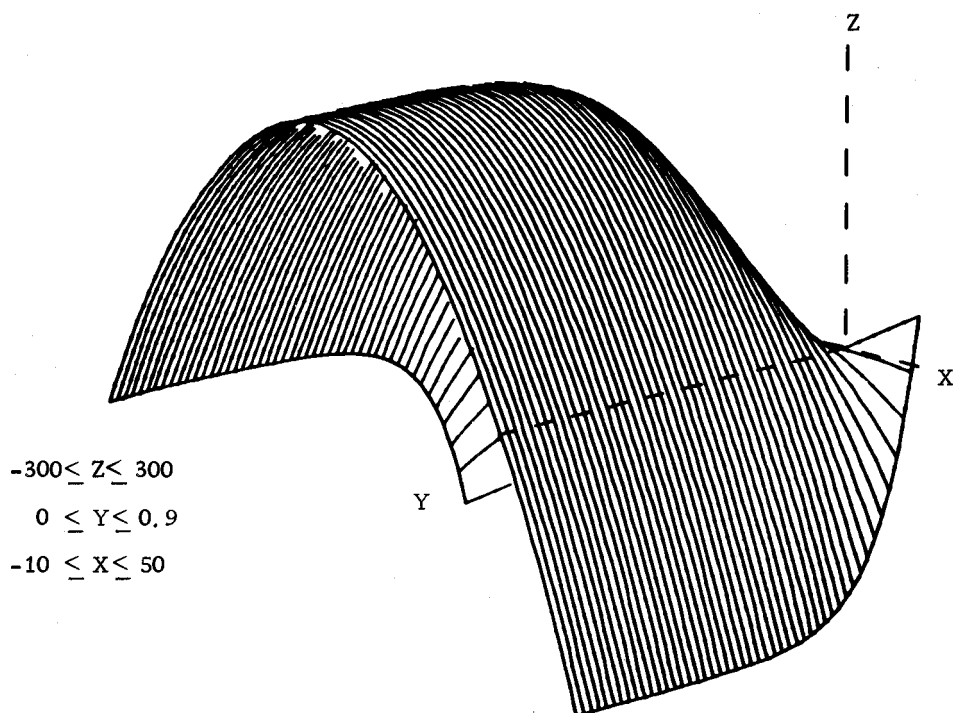
Figure 19. Estimation of respiration as function of temperature. Rs data extrapolated from hand-fit light curves.



PHOTOSYNTHESIS = F(LIGHT, TEMPERATURE)

Figure 20. Photosynthetic response (Z) to light (Y) and temperature (X).

$$Z = -5X + (391 - .457((X - 28.98)^2))(1 - e^{-10.05Y}) + .0012Y$$



PHOTOSYNTHESIS=F<LIGHT,TEMPERATURE> ; RESPIRATION LINEAR

Figure 21. Photosynthetic response (Z) to light (Y) and temperature (X).

$$Z = -5X + (391.3 - .457((X - 28.98)^2))(1 - e^{-10.05Y}) + .0012Y.$$

that forces the linear respiration term through the origin. The B_5 term is quite low (.0012) indicating that light saturation approaches a zero derivative asymptote. This suggests a minimum effect of shading on photosynthesis at high light intensities.

Figure 22 is a frequency distribution of the residuals for function (8). The distribution is skewed to the left which indicates that function to overestimate the data.

Addition of an intercept coefficient for respiration while dropping the "self-shading" coefficient (B_5) resulted in equation (9).

$$\text{Psn} = 115 - 13.8X + (551 - .53((X-36.2)^2))(1-e^{-10.8Y}) \quad (9)$$

A frequency distribution of the residuals (Figure 23) indicates a good fit of the function. However, the function predicts net CO_2 uptake at zero light for low temperatures which is inconsistent with the plant system although Walker (1971) has presented similar tentative findings using a Siemens cuvette system.

The respiration term was altered from a linear function to a symmetrical quadratic similar to that for net photosynthesis.

$$\text{Respiration} = B_0'' + B_1''((X-B_2'')^2)$$

B_0'' is the maximum respiration at temperature B_2'' . Since respiration is the CO_2 flux from the plant, B_0'' is a negative quantity and B_1'' is positive. Figure 24 shows the response surface for the following function considering maximum respiration to occur at B_2'' equal

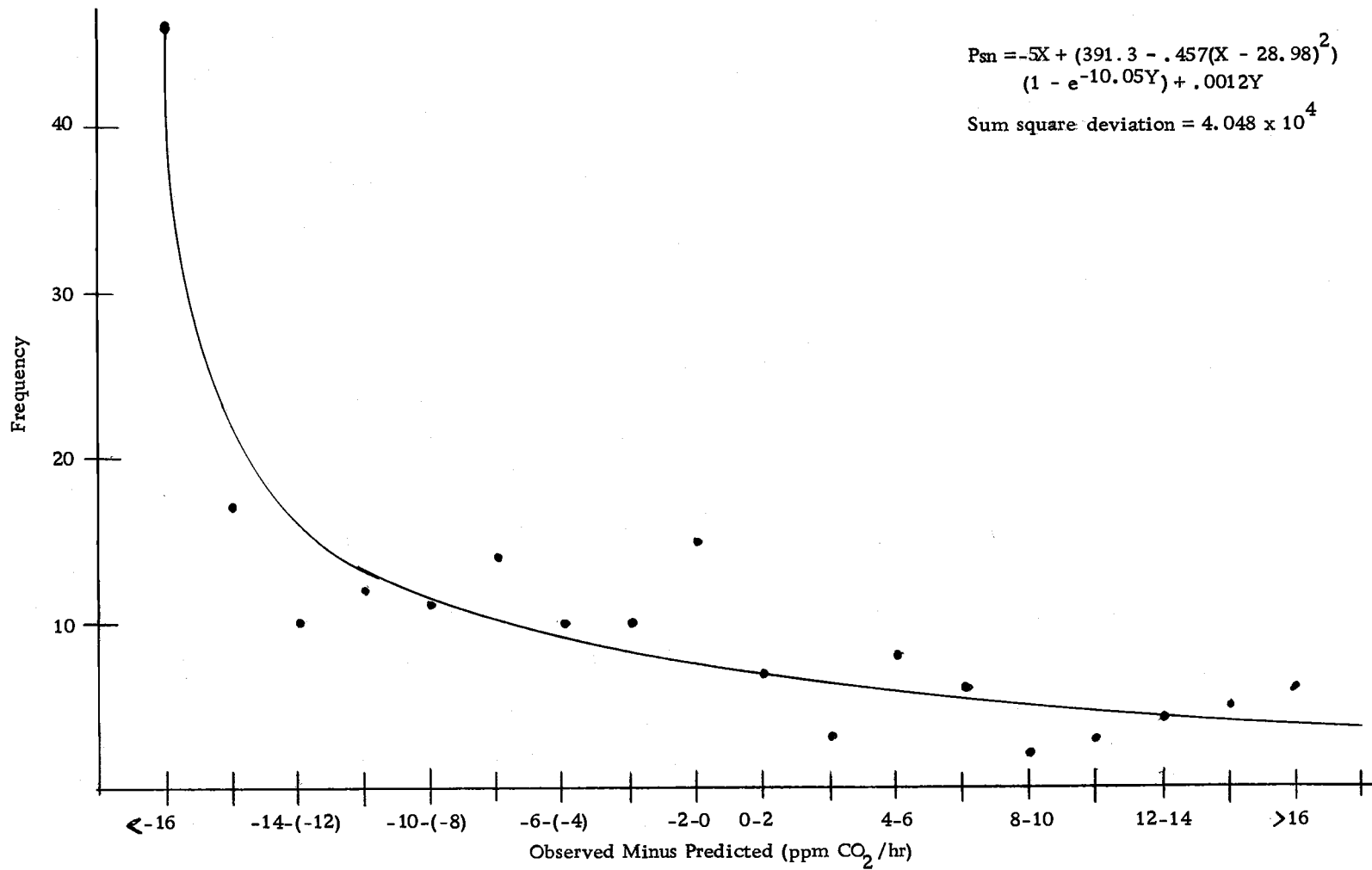


Figure 22. Frequency distribution of residuals for equation (8).

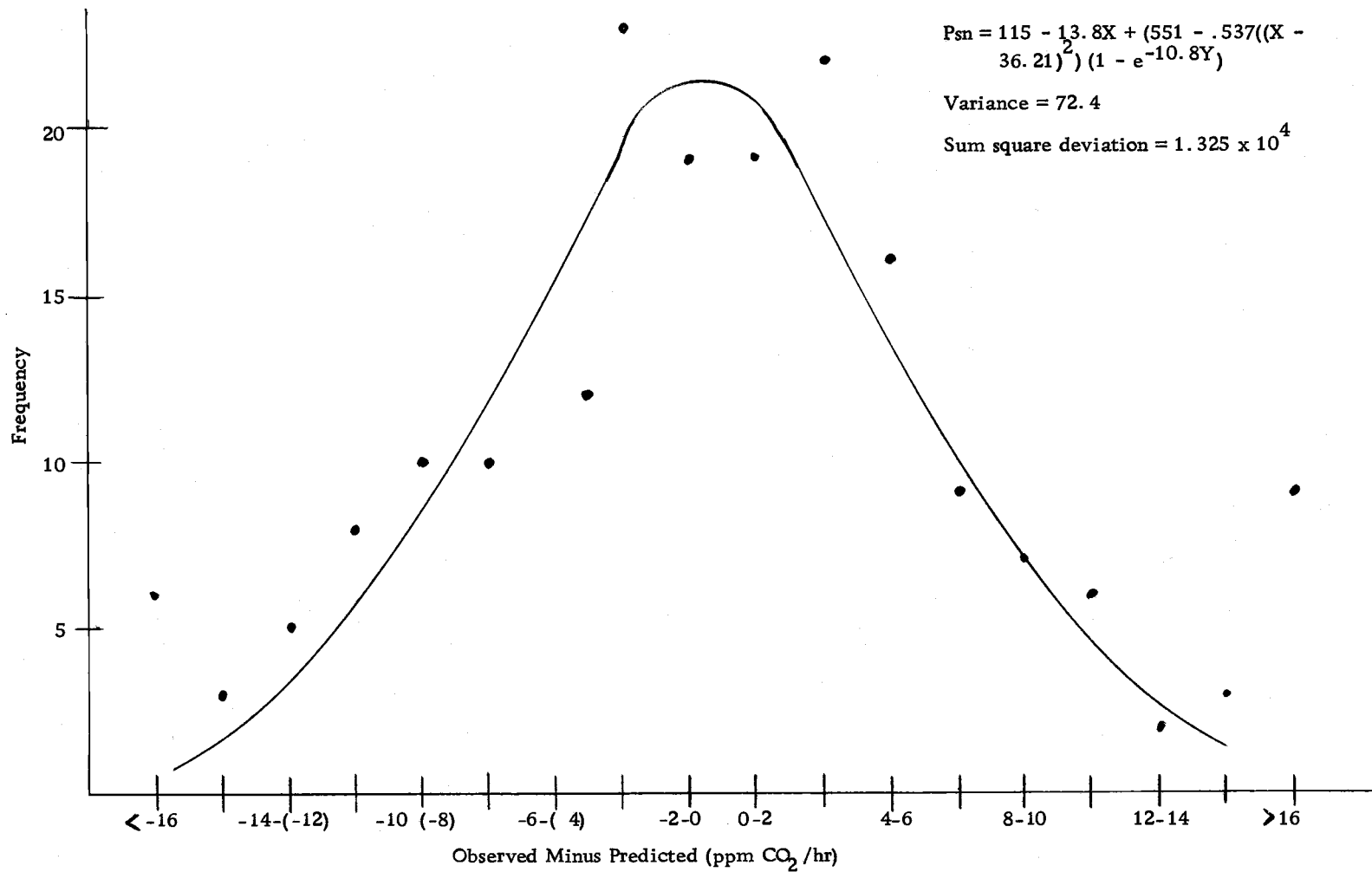
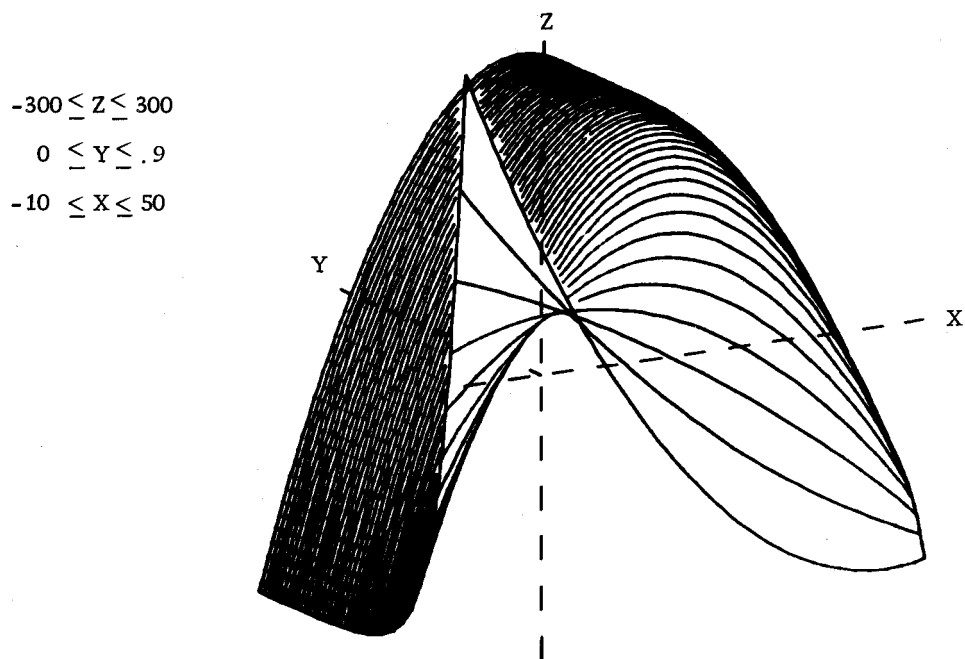


Figure 23. Frequency distribution of residuals; equation (9).



PHOTOSYNTHESIS = $F(\text{LIGHT}, \text{TEMPERATURE})$; RESPIRATION QUADRATIC

Figure 24. Photosynthetic response (Z) to light (Y) and temperature (X). Respiration is a quadratic function.

$$Z = (-294.7 + .22((X - 45.)^2)) + (472 - .775((X - 29.3)^2))(1 - e^{-10.49Y})$$

to 45°C:

$$P_{sn} = \frac{(-294.7 + .22((X-45)^2)) + (472 - .775((X-29.3)^2))}{(1 - e^{-10.49Y})} \quad (10)$$

For light levels below .05 ly/minute and temperatures below 7°C, the function predicts an unexpected increase in net photosynthesis. The same phenomenon can be observed in Figure 25 which shows the response surface resulting from a quadratic respiration function in which the temperature for maximum photosynthesis was held constant at 23.7°C. In addition, this function predicts abnormally high CO₂ uptake for low light levels at high temperatures. The frequency distribution of the residuals for (1) is normally distributed indicating the best fit of the function when using a least-squares criteria (see Figure 26).

Although the coefficient associated with the initial slope and the transition region of the light saturation curve is normally considered independent of temperature, it may be that this coefficient has some temperature dependence in a plant community system. The generalized expression can be written:

$$Z = f(X) + g(X)(1 - e^{h(X)Y}) \quad (11)$$

where

$$h(X) = B_0 + B_1((X - 23.7)^2)$$

A curvefit program that optimizes the fit of eight parameters

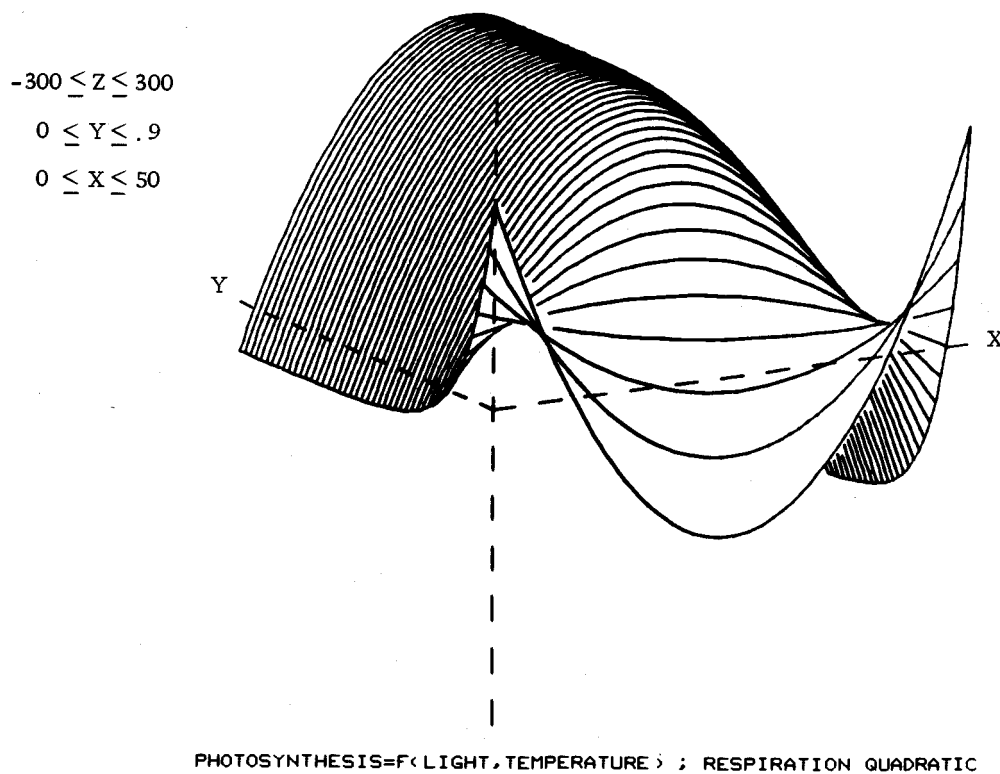


Figure 25. Photosynthetic response (Z) to light (Y) and temperature (X). Respiration is a quadratic function.

$$Z = (-156. + 58((X-29.8)^2)) + (408.2 - 1.17((X-23.7)^2))(1 - e^{-10.41Y})$$

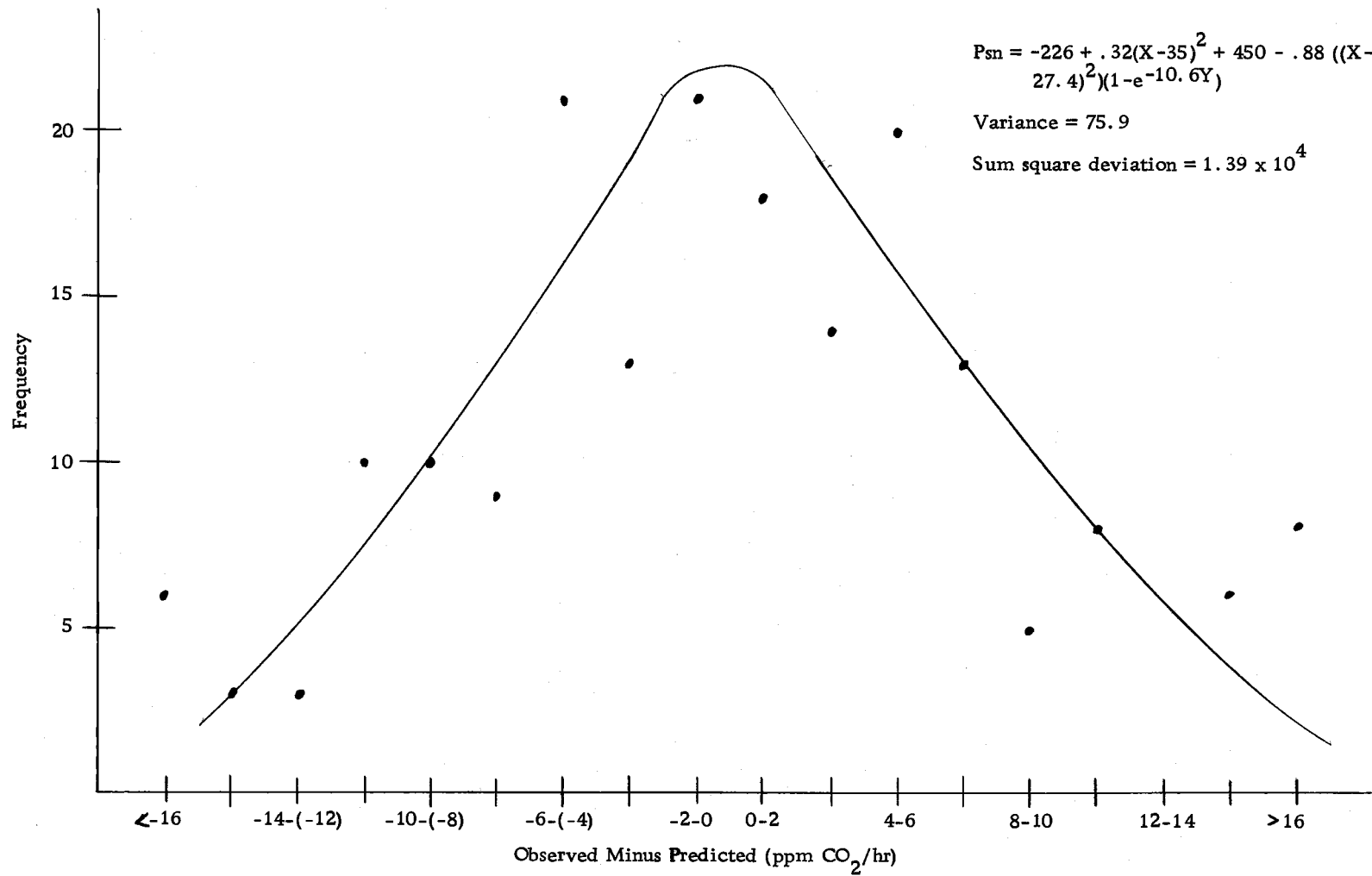


Figure 26. Frequency distribution of residuals for equation (10).

resulted in the following function:

$$P_{sn} = -328.4 + .16((X - 52.8)^2) + (474.3 - .709((X - 30)^2)) \\ (1 - e^{Y(10.45 - .007(X - 23.7)^2)}), \quad (12)$$

This function differs from the data by a weighted average of 3.7% (see residuals, Figure 27), but predicts net photosynthesis at zero light intensity for temperatures less than 8°C.

Experiment Three

Figure 28 shows the results from monitoring net photosynthesis for a 14-hour day compared to photosynthesis predicted from the stepwise regression equation (3). In almost all instances, the predicted exceeded the observed.

Figure 29 represents a comparison of the prediction accuracy between the stepwise equation (3) and the non-linear function (8) of non steady-state conditions. Both models overpredict net photosynthesis for the range of temperatures and radiation programmed for this 14-hour day. In general, the non-linear model seems the better predictor for this experiment. Note that the deviations between predicted and observed photosynthesis of the stepwise model are completely in phase with the deviations calculated from the non-linear model.

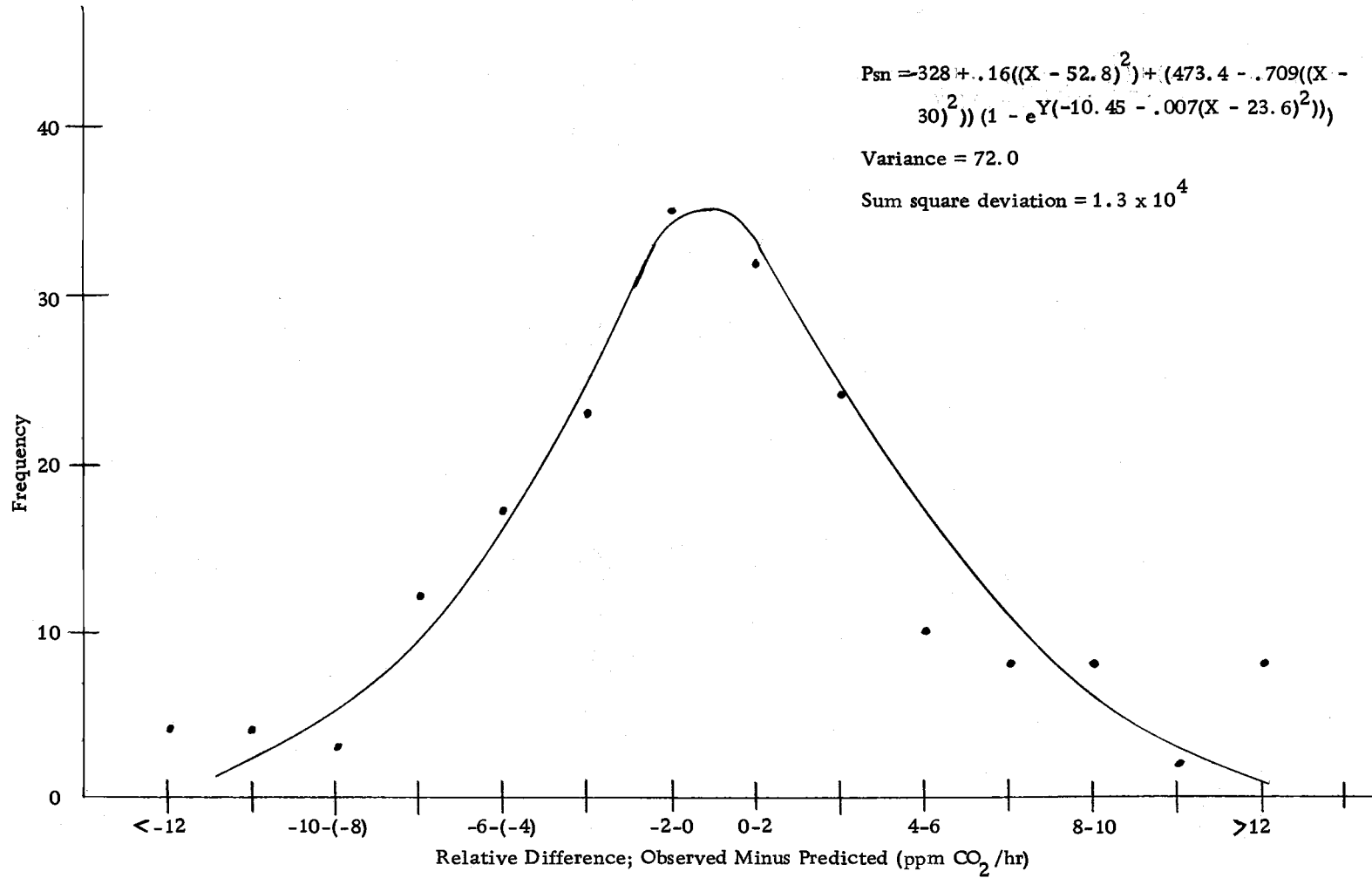


Figure 27. Frequency distribution of relative residuals for equation (12).

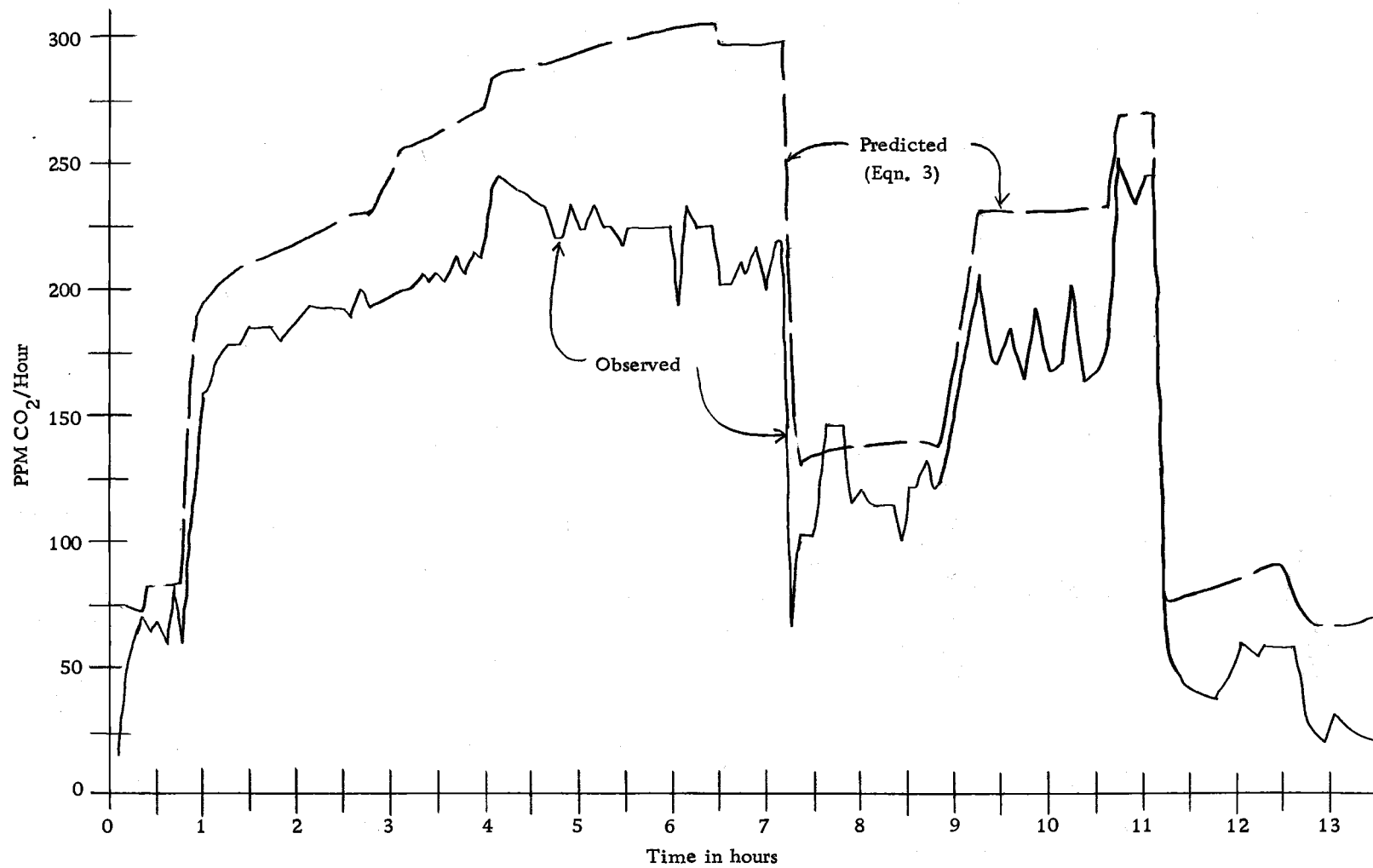


Figure 28. Net photosynthesis. Predicted and observed for 14-hour day.

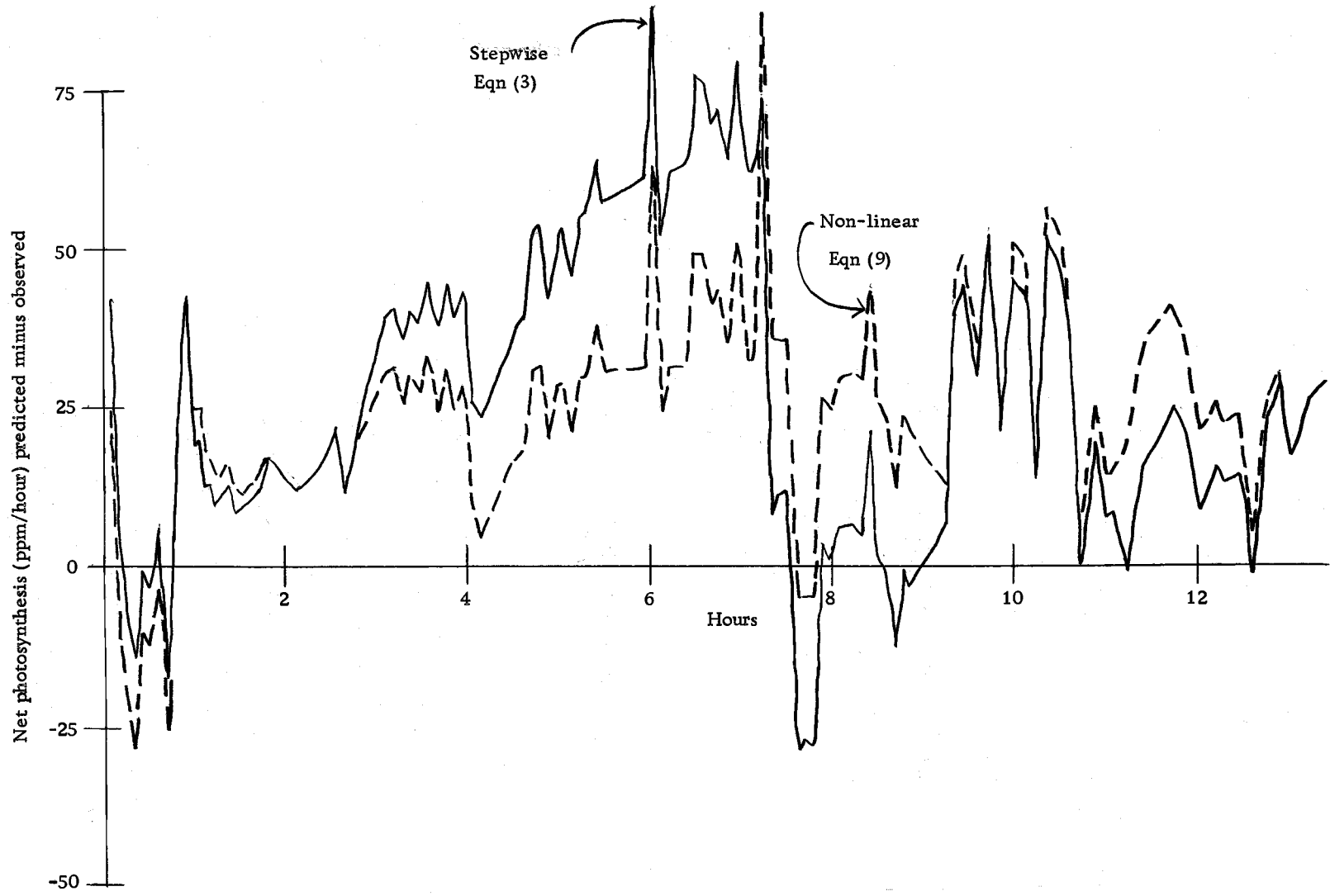


Figure 29. Comparison between stepwise and non-linear models as predictors of photosynthesis.

CONCLUSIONS

Both the non-linear and the stepwise models explicitly point out the nature of the interaction between temperature and light in predicting net photosynthesis. The explained variation in photosynthesis was increased significantly when multiplicative interaction terms of radiation and temperature were included in the stepwise analysis. The response surface of the non-linear model more clearly shows the logarithmic increase in temperature controlled photosynthesis as light energy increases. Comparative photosynthetic responses of various plant systems to light and temperature would be misleading without some measure of this interaction.

The prediction of net photosynthesis at zero light is an artifact that results from a lack of critical data. Since there are no data below 6° and because there are no photosynthetic data at very low light levels, the function that predicts respiration is weighted by the curve-fit program at temperatures above 6° . The only way to force the respiration function to conform to the known photosynthetic response is to fix the algebraic sign of the coefficients. This was done in equation (1) with the resulting biased fit of the data as seen in the skewed distribution of the residuals. Additional work is needed before the model can be extended to low light levels (5% full sunlight) at temperatures below 6° .

The non-linear equation (12) predicts net photosynthesis within a weighted average of $\pm 3.7\%$. This excellent fit coupled with the known physiological responses associated with the coefficients indicates that the model is structurally reliable. However, additional variables are needed before net photosynthesis can be used to predict primary productivity so the model can be field tested. The photosynthetic response to preconditioning, plant moisture stress, and vegetation density are the most important independent variables that require future work. The computer-linked controlled environment system that was developed as a part of this project can be a powerful tool for collecting the large quantities of data needed to model these additional response functions.

BIBLIOGRAPHY

- Atlas Electric Devices Company. 1969. Atlas fade-ometer and weather-ometer. Chicago. 32 p.
- Belehradek, Jan. 1957. A unified theory of cellular rate processes based upon an analysis of temperature action. *Protoplasm* 48: 53-71.
- Cleary, Brian D. 1971. The effect of plant moisture stress on the physiology and establishment of planted Douglas-fir and ponderosa pine seedlings. Ph. D. thesis. Corvallis, Oregon State University. 85 numb. leaves.
- Ferrell, W. K. Variation in photosynthetic efficiency within forest tree species. First North American Forest Biology Workshop. East Lansing, Michigan. August 5-7, 1970. In press.
- Forward, Dorothy F. 1960. Effect of temperature on respiration. In: *Encyclopedia of plant physiology*. Berlin, Springer-Verlag. p. 239-258.
- Gaastri, P. 1963. Climatic control of photosynthesis and respiration. In: *Environmental control of plant growth*. L. T. Evans (ed.). New York, Academic. p. 113-138.
- Heath, O. V. S. 1969. The physiological aspects of photosynthesis. London, Heinemann Educational Books Limited. 309 p.
- Kramer, Paul J. and T. T. Kozlowski. 1960. *Physiology of trees*. New York, McGraw-Hill. 640 p.
- Krueger, K. W. and R. H. Ruth. 1969. Comparative photosynthesis of red alder, Douglas fir, and Sitka spruce, and western hemlock seedlings. *Canadian Journal of Botany* 47(4):519-527.
- Langriege, J. 1963. Biochemical aspects of temperature response. In: *Annual review of plant physiology* 14:441-462.
- Larcher, W. 1969. Physiological approaches to the measurement of photosynthesis in relation to dry matter production by trees. *Photosynthetica* 3(2):150-166.
- Ledig, F. T. and Thomas O. Perry. 1969. Net assimilation rate and growth in loblolly pine seedlings. *Forest Science* 15(4):431-438.

- Ledig, F. T. 1969. A growth model for tree seedlings based on the rate of photosynthesis and the distribution of photosynthate. *Photosynthetica* 3(3):263-275.
- Lewis, J. K. 1970. Primary producers in grassland ecosystems. In: *The grassland ecosystem*, R. L. Dix and R. G. Beidleman (eds.). Range Science Department Science Series No. 2. Fort Collins, Colorado State University. p 1-87. (supplement)
- Loomis, R. S., W. A. Williams and W. G. Duncan. 1967. Community architecture and the productivity of terrestrial plant communities. In: *Harvesting the sun. Photosynthesis in plant life*. Anthony San Pietro (ed.). New York, Academic.
- Milner, Harold W. and William H. Hiesey. 1969. Photosynthesis in climatic races of Mimulus. I. Effect of light intensity and temperature on rate. *Plant Physiology* 39(2):208-213.
- Moir, W. H. 1969. Energy fixation and the role of primary producers in energy flux of grassland ecosystems. In: *The grassland ecosystem, a primary synthesis*. R. L. Dix and R. G. Beidleman (eds.). Range Science Department Science Series No. 2. Fort Collins, Colorado State University. p. 125-148.
- Pisek, Van Arthur et al. 1969. Kardinale Temperaturbereiche der Photosynthese und Grenztemperaturen des Lebens der Blätter Verschiedener Spermatophyten. III. Temperaturabhängigkeit und Optimaler Temperaturbereich der Netto-photosynthese. *Flora* 158:608-630.
- Rabinowitch, Eugene I. 1951. Photosynthesis and related processes. Vol. 2, part 1. New York, Interscience. p. 603-1208.
- _____ 1956. Photosynthesis and related processes. Vol. 2, part 2. New York, Interscience. p. 1211-2088.
- _____ 1969. Photosynthesis. New York, Wiley. 273 p.
- Saieki, Toshiro. 1963. Light relations in plant communities. In: *Environmental control of plant growth*. L. T. Evans (ed.). New York, Academic. p. 79-92.
- Schulze, Von Ernst-Detlef. 1970. Der CO₂-Gaswechsel der Buche (Fagus silvatica L.) in Abhängigkeit von den Klimofaktoren im Freiland. *Flora* 159:177-232.

- Stalfelt, M. G. 1960. Temperatur. In: Encyclopedia of Plant Physiology. Vol. 2. Berlin, Springer-Verlog. p. 100-118.
- Strain, B. R. and V. C. Chase. 1966. Effect of past and prevailing temperatures on the CO₂ exchange capacities of some woody desert perennials. Ecology 47(6):1043-1045.
- Walker, Richard B. and David J. Salo. 1971. Low temperature assimilation in Douglas-fir. Northwest Scientific Association meeting. Moscow, Idaho. April 16-17.

APPENDIX

The controlled environment system was characterized prior to experimentation with plant systems. The data and experimental methods are described.

The system was tested for leaks by increasing the chamber CO₂ concentration to 80 ppm above that of ambient concentration. Normal environmental conditions were established and the rate of CO₂ decrease measured with the gas analyzer. To localize any leaks, the system was pressurized to 1 cm of water with 20% Freon-12. Leakage was determined with an electronic thermalconductivity cell and leaks plugged with silicone sealant. The system was similarly leak tested prior to placing plants in the chamber for each experiment. The ambient CO₂ concentration was determined prior to each experiment and held constant by simply opening the laboratory door to the outside air.

Light spectra were measured with an ISCO spectroradiometer, model SR. The instrument was recalibrated every three weeks with a quartz-iodine lamp calibrated by the National Bureau of Standards. The output from the radiometer was digitized onto paper tape and relayed to the computer for processing. The relative spectrum was checked at several points in the chamber and found to be constant. Several of these spectra are on pages 68 and 69. A computer program was prepared to integrate the spectra to obtain measurements on the light energy available between any two wave lengths. Some of these data appear on page 70.

Spectra for lamp filters were determined and appear on page 71. Spectra for several combinations of filters appear on page 72. In general, all light filters tend to have a constant percent transmission in all wave bands except in the ultraviolet.

As the xenon arc aged, darkening appeared in one-half inch

bands next to both electrodes. Also, considerable spattering of the tungsten electrodes caused a thin white film to form on 50 to 70% of the inner surface of the burner tube. This caused a 15% decrease in output in the first 100 hours and a slower rate (2%/100 hours) thereafter.

Measurements of light uniformity were made with a Kipp solarimeter whose output was taken on a microvolt meter. Data were taken for three different horizontal planes and at nine points within each plane. The data appear in Table 7 on page 74. Horizontal uniformity is within 15% and the usual decrease in energy as a function of distance from the light source is observed.

Temperature uniformity was determined by locating seven thermopiles at various points throughout the chamber (see Table 8, page 75). The output was digitized onto paper tape with the data acquisition system and the millivolt signal reduced to degrees C with a computer program. The data were taken with lights off since high radiation loads necessitated that the thermocouples be thoroughly shielded and insulated to obtain reproducible temperature data. The data indicate uniformity to be within 1°C and that chamber temperature is within 1°C of that programmed.

The accuracy of the cam programmer was determined by cutting the cam to produce a sine wave with a 24-hour period, and monitoring the temperature in the center of the chamber at ten minute intervals for 24 hours with an electric psychrometer. Millivolt output from the psychrometer was digitized and reduced to degrees C. The graph on page 76 shows the chamber temperature and the programmed temperature for a 24-hour period. In only one instance did the chamber temperature deviate from the programmed temperature by more than 1°C .

Vapor pressure uniformity was not rigorously tested since a constant temperature profile assures a constant vapor pressure

profile in a closed system. The accuracy of a cam programmer for wet bulb depression was determined simultaneously with dry bulb temperature. The results appear on page 77. The graph shows that for the morning hours from 7 to 11 AM, wet bulb depression was less than that programmed. This is due to an excessive accumulation of the cooling coil during high relative humidities during the night. The water vapor precipitator was inadequate to remove large volumes of water from the system during short time periods thus causing increased humidities. Once the cooling coil was dried, the wet bulb depression was maintained within 1°C of the programmed wet depression.

The air velocity profile was measured with a Thornwaite anemometer. The data are presented in Table 9 on page 78.

The CO_2 control system can be evaluated by referring to the graph on page 79. Pulse height is reproducible within 5 to 10% and mixing within the chamber occurs within ten seconds.

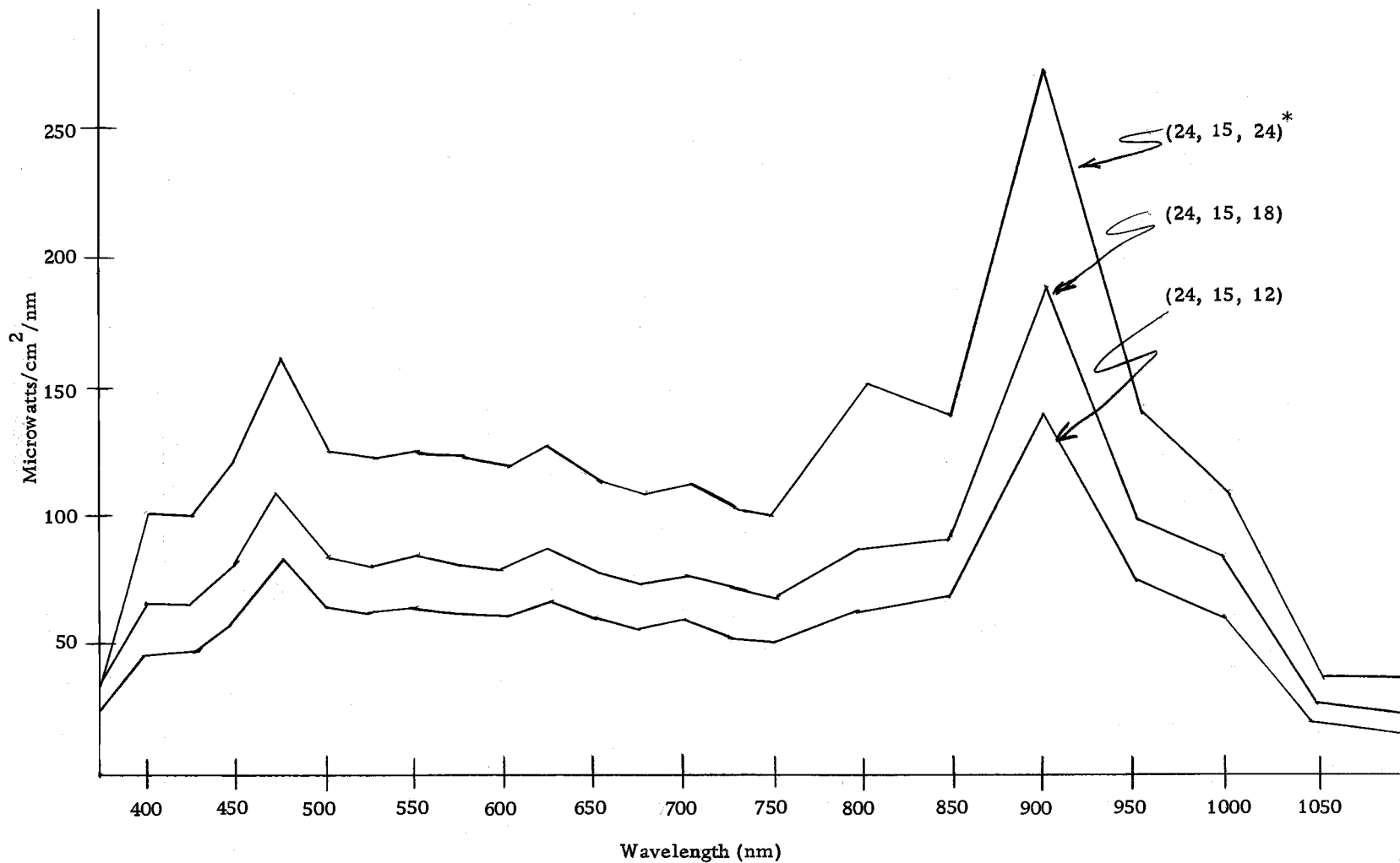


Figure 30. Xenon arc spectra at 12", 18", and 24" from floor, center of chamber. (*Refers to inches from a reference point [0,0,0] in the standard X, Y, Z coordinates. Reference point is lower front corner of chamber near supply air plenum.)

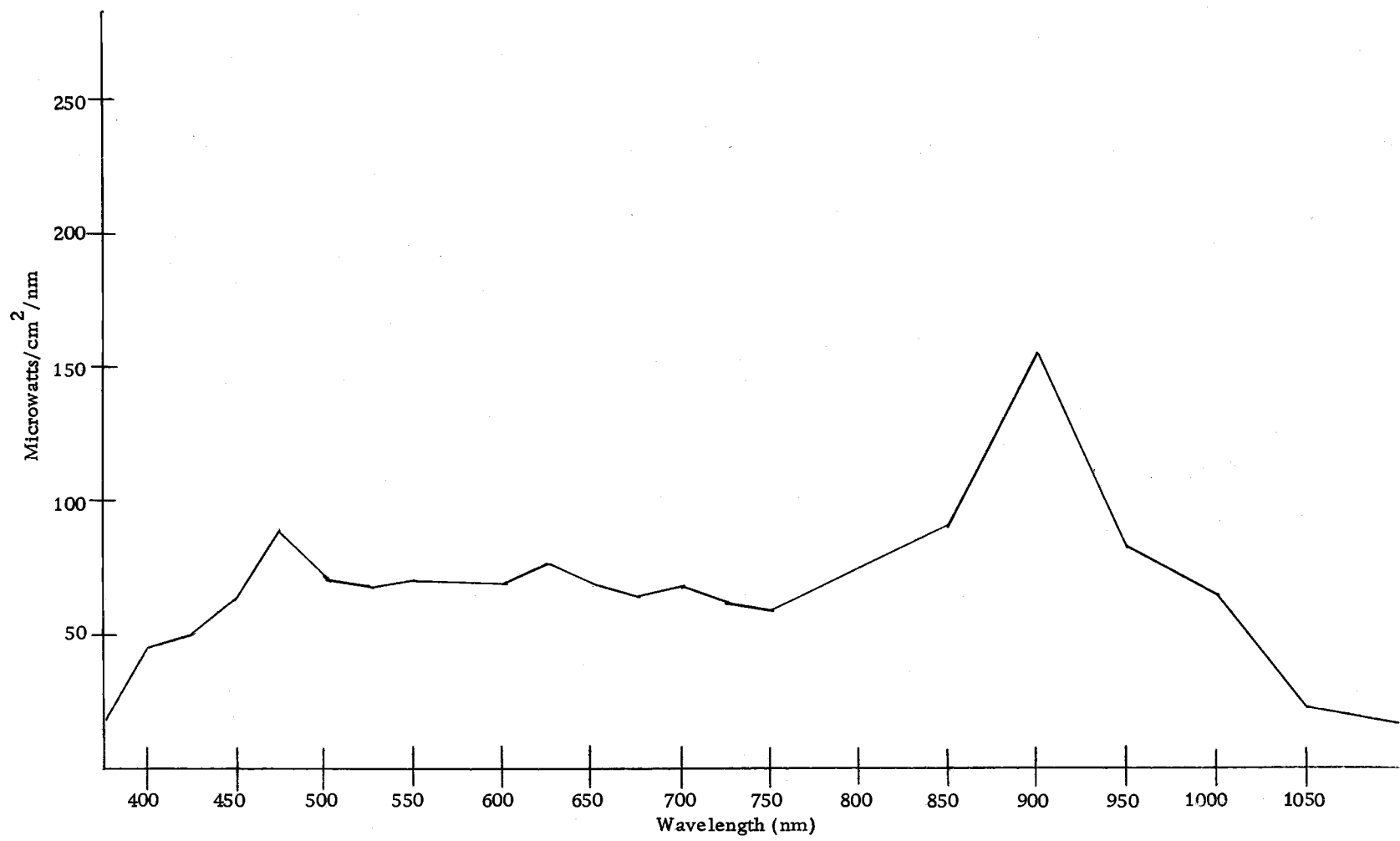


Figure 31. Xenon arc spectrum 12" from floor near one end of chamber.

Table 5.* Energy distribution between visible and infrared spectra of xenon arc.

| Position in chamber** | Waveband | Microwatts / cm ² | Ly/min | % Visible / total |
|-----------------------|----------|------------------------------|--------|-------------------|
| 24, 15, 12 | 375-725 | 20363 | 0.29 | 45.3 |
| | 725-1100 | 24351 | 0.35 | |
| 24, 15, 18 | 375-725 | 26913 | 0.38 | 44.7 |
| | 725-1100 | 32597 | 0.47 | |
| 24, 15, 12 | 375-725 | 39532 | 0.57 | 45.8 |
| | 725-1100 | 47546 | 0.68 | |

* Data from integration of spectra, Figure 31.

** Refers to inches from a reference point (0, 0, 0) in the x, y, z coordinate system. Reference point is lower front corner of chamber near supply air plenum.

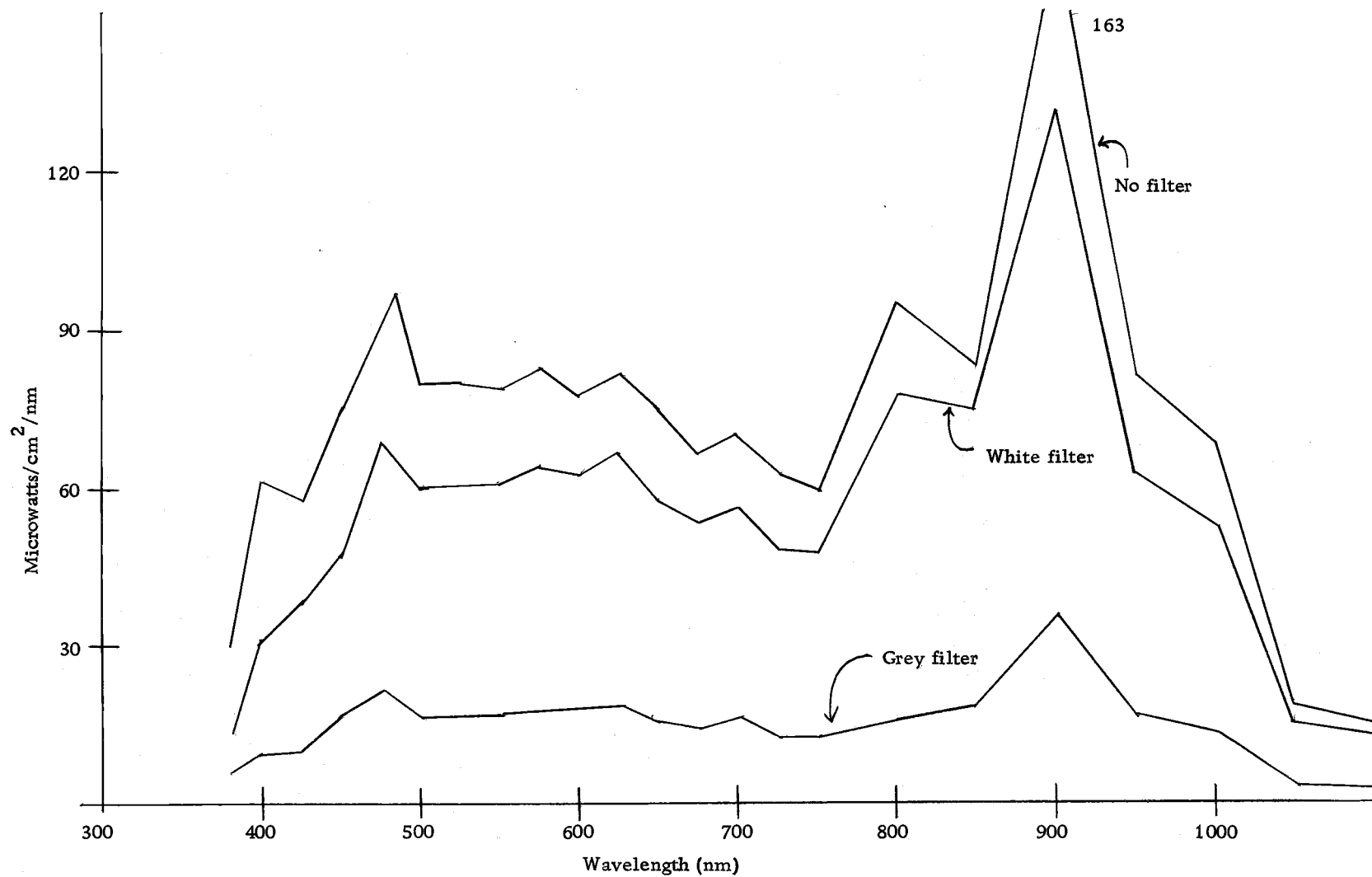


Figure 32. Radiation transmission spectra of xenon arc for white and grey filters.

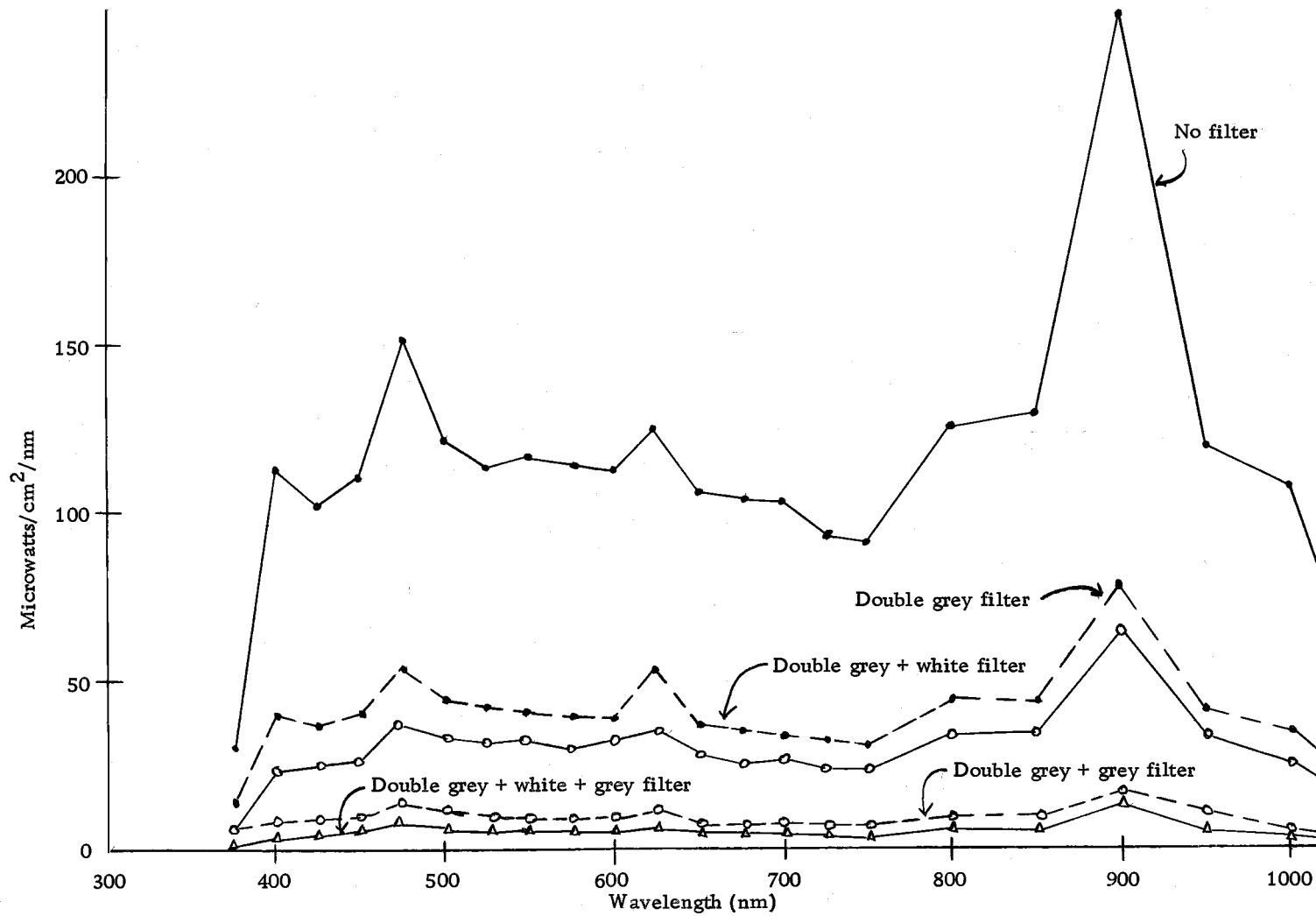


Figure 33. Spectra transmission for several chamber filters.

Table 6. Short-wave radiation transmission of xenon arc for several filter combinations, 18" from floor.

| Filter combination | mV | Ly/min |
|----------------------------|------|--------|
| All | 0.22 | .025 |
| Double grey + grey + white | 0.41 | .043 |
| White + grey + single grey | 0.76 | .081 |
| Grey + white | 1.33 | .142 |
| Grey | 1.62 | .173 |
| Double + single grey | 1.65 | .176 |
| Double grey + white | 1.82 | .194 |
| Double grey | 2.28 | .243 |
| White + single grey | 3.36 | .358 |
| Single grey | 4.14 | .441 |
| White | 5.82 | .619 |
| None | 7.43 | .790 |

Table 7. Radiation uniformity in the environment chamber.

| Position of radiometer* x, y, z (inches) | mV | Langleys |
|---|------|----------|
| 24, 15, 18 | 7.2 | .77 |
| 4, 15, 18 | 7.0 | .75 |
| 44.5, 15, 18 | 7.2 | .77 |
| 44.5, 3.5, 18 | 7.5 | .80 |
| 44, 25, 18 | 7.0 | .75 |
| 24, 27, 18 | 6.9 | .73 |
| 24, 5, 18 | 6.6 | .69 |
| 4, 27, 18 | 5.9 | .61 |
| 10, 27, 18 | 7.6 | .81 |
| 3.5, 3, 18 | 7.3 | .78 |
| 3.5, 3, 24 | 8.1 | .86 |
| 3.5, 15, 24 | 7.8 | .83 |
| 3.5, 27, 24 | 7.4 | .78 |
| 11, 27, 24 | 8.1 | .86 |
| 24, 27, 24 | 8.2 | .87 |
| 24, 15, 24 | 10.5 | 1.12 |
| 24, 6.5, 24 | 8.6 | .91 |
| 44, 4.5, 24 | 7.6 | .81 |
| 44, 15, 24 | 8.1 | .86 |
| 44, 27, 24 | 7.5 | .80 |
| 24, 15, 12 | 5.5 | .59 |
| 24, 26, 12 | 5.7 | .60 |
| 24, 4, 12 | 5.3 | .57 |
| 4, 26, 12 | 6.4 | .68 |
| 4, 15, 12 | 6.7 | .71 |
| 4, 4, 12 | 6.6 | .20 |
| 44, 15, 12 | 7.1 | .75 |
| 44, 26, 12 | 6.5 | .69 |
| 44, 4, 12 | 7.2 | .77 |

* Reference 0, 0, 0 is the lower front corner near the supply air plenum.

Table 8. Temperature uniformity in environment chamber.

| Programmed temp. (°C) | Actual temperature | | | | | | |
|-----------------------------|---------------------|------------|------------|-----------|------------|------------|-----------|
| | Position (x, y, z)* | | | | | | |
| | 4, 15, 18 | 24, 15, 18 | 44, 15, 18 | 24, 4, 18 | 24, 22, 18 | 24, 15, 36 | 29, 15, 4 |
| 16 | 15.9 | 16.3 | 15.9 | 16.7 | 16.8 | 16.3 | 16.6 |
| 20 | 20.6 | 21.0 | 20.5 | 20.9 | 21.3 | 20.1 | 19.6 |
| 25 | 25.5 | 25.4 | 25.5 | 25.5 | 25.5 | 25.7 | 25.9 |
| 30 | 30.1 | 29.5 | 30.3 | 29.5 | 29.2 | 30.2 | 30.4 |
| 35 | 35.4 | 34.5 | 35.8 | 34.3 | 34.1 | 35.6 | 36.0 |

* Reference position (0, 0, 0) is at the lower front near the supply air plenum.

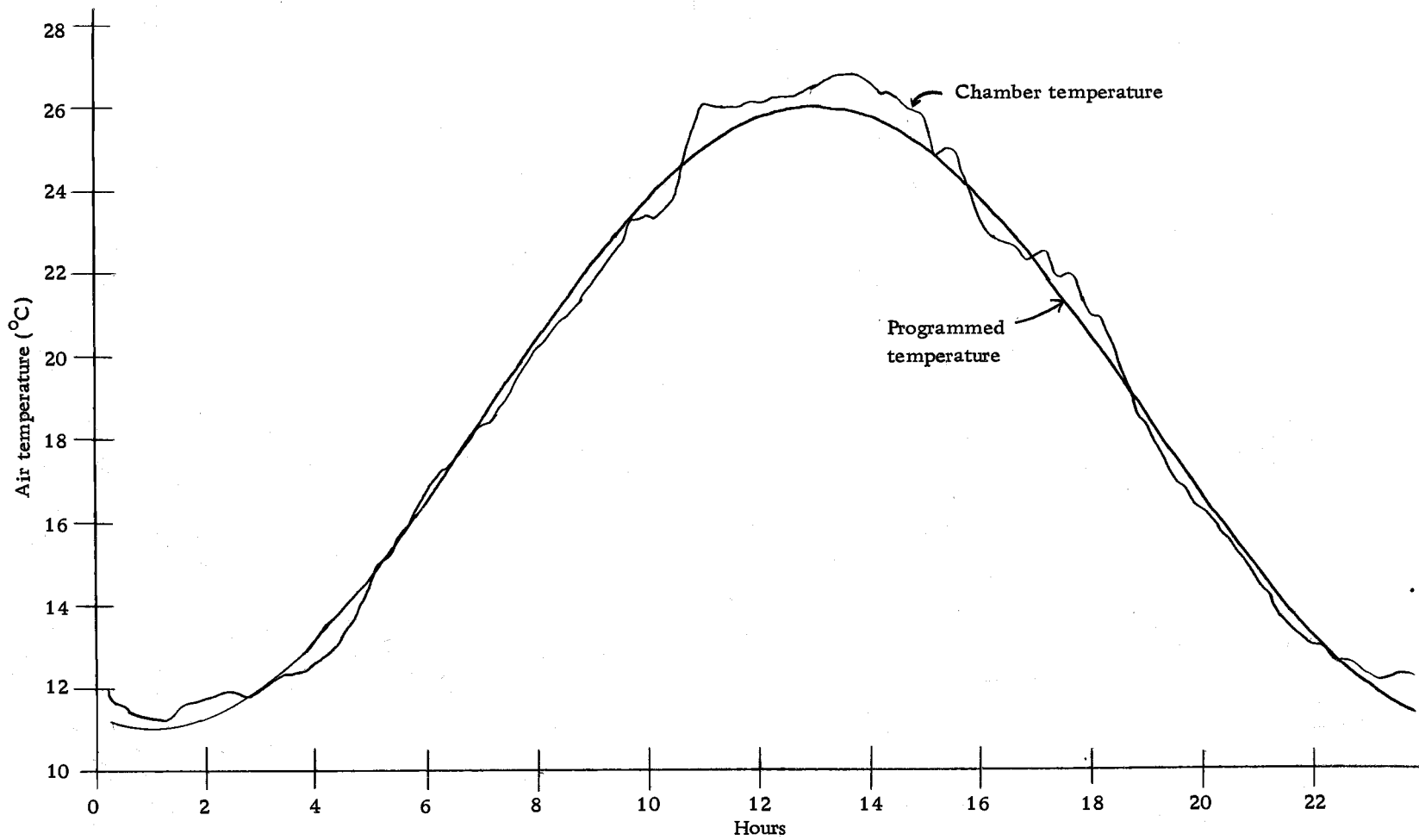


Figure 34. Comparison of actual chamber temperature and the temperature pattern programmed onto the cam programmer.

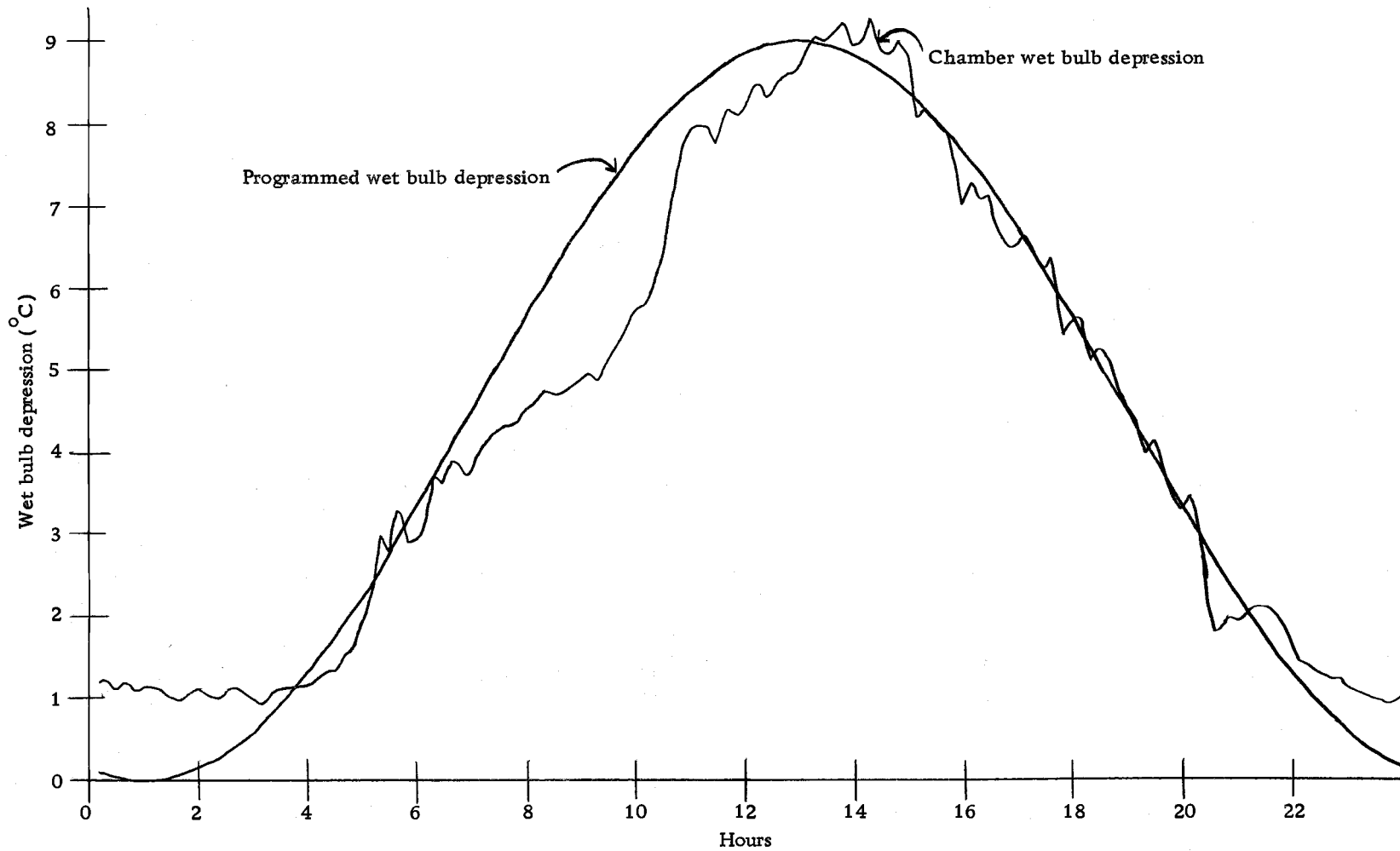


Figure 35. Comparison of chamber wet bulb depression with pattern programmed on cam programmer.

Table 9. Air velocities in chamber.

| Anemometer position* | mph | m/sec |
|----------------------|------|-------|
| 24, 15, 18 | 1.3 | .582 |
| 24, 15, 9 | 1.5 | .671 |
| 24, 15, 24 | 1.85 | .827 |
| 4, 15, 9 | 2.8 | 1.25 |
| 44, 15, 9 | 1.2 | .537 |

* Reference position (0, 0, 0) is lower front of chamber near supply air plenum.

Table 10. Nutrient solution used for red alder.

| <u>Chemical</u> | <u>Molar concentration</u> |
|-----------------------|----------------------------|
| K_2SO_4 | 0.0016 |
| $HgSO_4 \cdot 7H_2O$ | 0.002 |
| KH_2PO_4 | 0.00017 |
| K_2HPO_4 | 0.00083 |
| $CaSO_4 \cdot H_2O$ | 0.006 |
| $CaCl_2$ | 0.0005 |
| NH_4NO_3 | 0.001 |
| <u>Microelements</u> | <u>ppm</u> |
| H_3BO_4 | .25 |
| $MnSO_4 \cdot 4H_2O$ | .05 |
| $ZnSO_4 \cdot 7H_2O$ | .05 |
| $CuSO_4 \cdot 5H_2O$ | .02 |
| $NaMoO_4 \cdot 2H_2O$ | .01 |
| FeEDDHA | 1.0 |

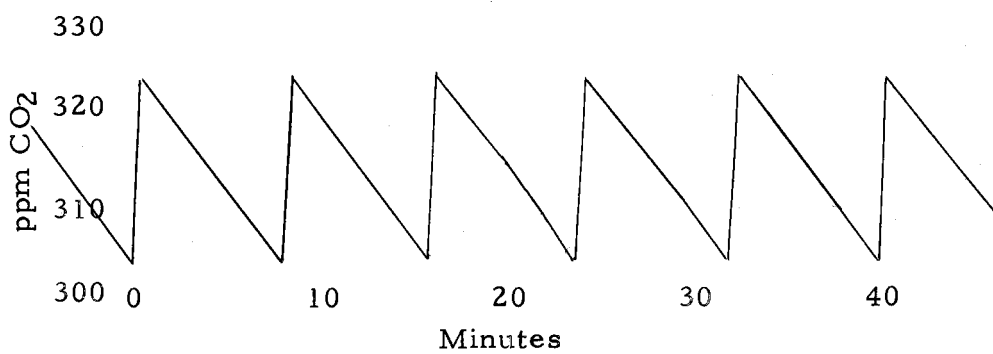


Figure 36. Record of CO₂ depletion and resupply in environment chamber.